Forschungszentrum Karlsruhe
Technik und Umwelt
Wissenschaftliche Berichte
FZKA 6598

Detailed FE-Analysis of the LCT-coil with Input of Displacements (version Nr. 3) taken from the Global Model of the Configuration with the TFMC

A. Grünhagen
Institut für Medizintechnik und Biophysik
Projekt Kernfusion

Juni 2001

Forschungszentrum Karlsruhe

Technik und Umwelt

Wissenschaftliche Berichte

FZKA 6598

Detailed FE-Analysis of the LCT-coil with input of displacements (version Nr. 2) taken from the global model of the configuration with the TFMC

A. Grünhagen

Institut für Medizintechnik und Biophysik

Projekt Kernfusion

Forschungszentrum Karlsruhe GmbH, Karlsruhe

2001

Forschungszentrum Karlsruhe GmbH
Postfach 3640, 76021 Karlsruhe

Mitglied der Hermann von Helmholtz-Gemeinschaft
Deutscher Forschungszentren (HGF)

ISSN 0947-8620

Detailierte FE-Analyse der LCT-Spule mit vorgeschriebenen Verschiebungen (Version Nr. 2) aus der globalen Model-Konfiguration zusammen mit der TFMC

Zusammenfassung

Für die Entwicklung von ITER-Magneten ist das Testen einer TF-Modellspule in einer Konfiguration mit der LCT-Spule in der TOSKA-Anlage eine wichtige Vorbereitungsstufe. In diesem Versuchsaufbau muss auch die mechanische Zuverlässigkeit der LCT-Spule gewährleistet sein. Die Festigkeitsberechnungen mit dem Finite-Element-Programm ABAQUS zu dieser Spule zeigen ein unkritisches Verhalten der LCT-Struktur.

Abstract

For the development of ITER magnets, the testing of a TF model coil in the TOSKA facility is an important preliminary step. The test configuration consists of the model coil and the LCT coil. The mechanical reliability of the LCT coil has to be guaranteed in this experiment assembly. The strength calculations of this coil with the finite-element program ABAQUS show an uncritical behaviour of the LCT structure.

Contents

1. Introduction

The construction of the **TF** (**T**oroidal **F**ield) model coil is a major item of the R&D program for the **ITER** magnets. The main objectives of the **TF** **M**odel **C**oil (**TFMC**) are to demonstrate the:

- feasibility of the manufacturing processes
- reliability of the integrated system

Most of the manufacturing processes require testing before use in a full size coil, in particular the joints, the radial plates, the insertion of the conductor into the grooves, heat treatment, transfer, insertion of winding pack into casing. Of course, separate tests will be performed for each item, but the feasibility of the whole concept will only be demonstrated by manufacturing a model including all different features of the coil.

The test of an integrated system is the only way to fully qualify the different techniques used during the manufacture. The extensive test program must be representative concerning the constraints which occur in the real device. Furthermore, the test should be able to evaluate the safety margins of the parameters investigated.

In the test configuration the TFMC is positioned adjacent to the LCT coil under an angle of 4.5 degrees (figures 1 and 2) in the TOSKA facility at the Forschungszentrum Karlsruhe.

2. Finite Element Analysis

2.1 Objective

The assembly of the test configuration consists of the TFMC (winding, casing, and support structure), intercoil structure, and the LCT coil (figures 1 and 2). The magnetic field computed with EFFI /1/ is 9.64 T for a current I=80 kA of the TFMC winding and I=16 kA for the LCT winding. The D-shaped LCT coil produces the magnetic background field for the test with the TFMC. The coil systems in the TOSKA reference coordinate system are subject to an attraction force (out-of-plane) of F_y=82.6 MN and an in-plane force of F_x=14.6 MN. The intercoil structure connects both coils and provides for the transfer of the in-plane and out-of-plane forces. The attraction forces are transmitted by a set of five horizontal plates inserted between the steel belts of the LCT-coil. Three upper and three lower belts of the original twelve steel belts are removed. From the remaining outer-most lower and upper belt, one inner half belt was removed, too for increasing the thickness of the two outer-most horizontal plates. Over the whole width, two pads positioned at the top and at the bottom of the LCT casing are also utilised for the transmission of these forces. The in-plane forces are transferred by two hooks situated at the outer corners of the LCT casing. Furthermore, the five horizontal plates have hooks resting on the LCT casing side plate. The hooks will also be used for the transmission of the in-plane forces.

The behaviour of the LCT coil in this assembly is of great interest. The calculations of the deformations and the stresses are performed by the **F**inite **E**lement **M**ethod (**FEM**) with the program system ABAQUS /2/.

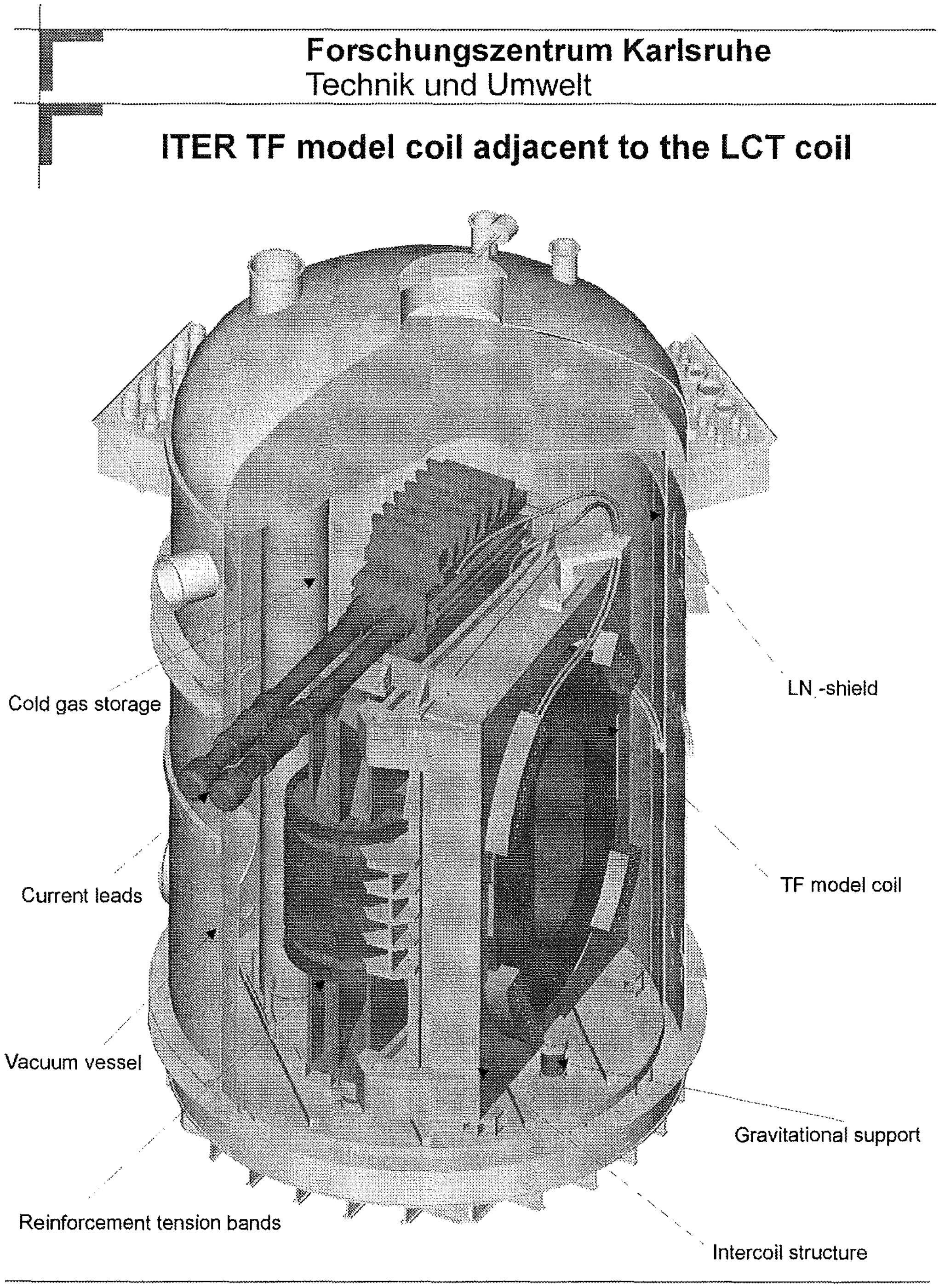

Figure 1 - LCT-ITER TF model coil configuration in TOSKA

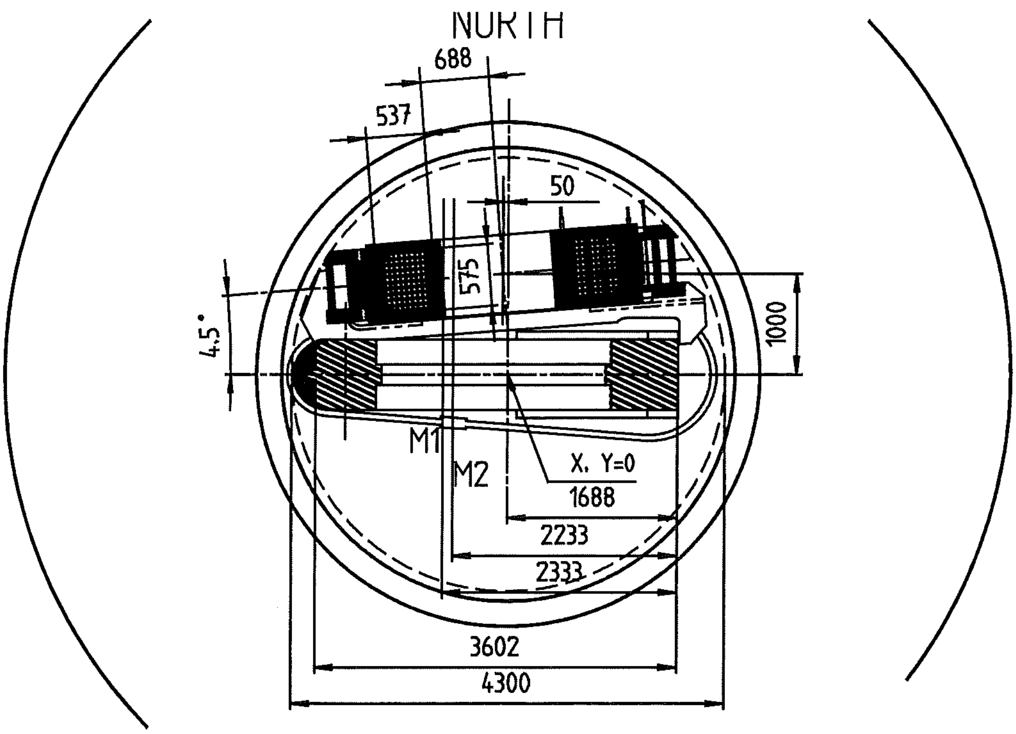

Figure 2 - Top view of the LCT-ITER TF model coil configuration in TOSKA

2.2 Model Description

For structure analyses of the LCT coil, an existing FE model /3/ was used. A complete FE model with this detailed LCT model has not been developed. Figure 3 shows the FE model of the LCT-coil.

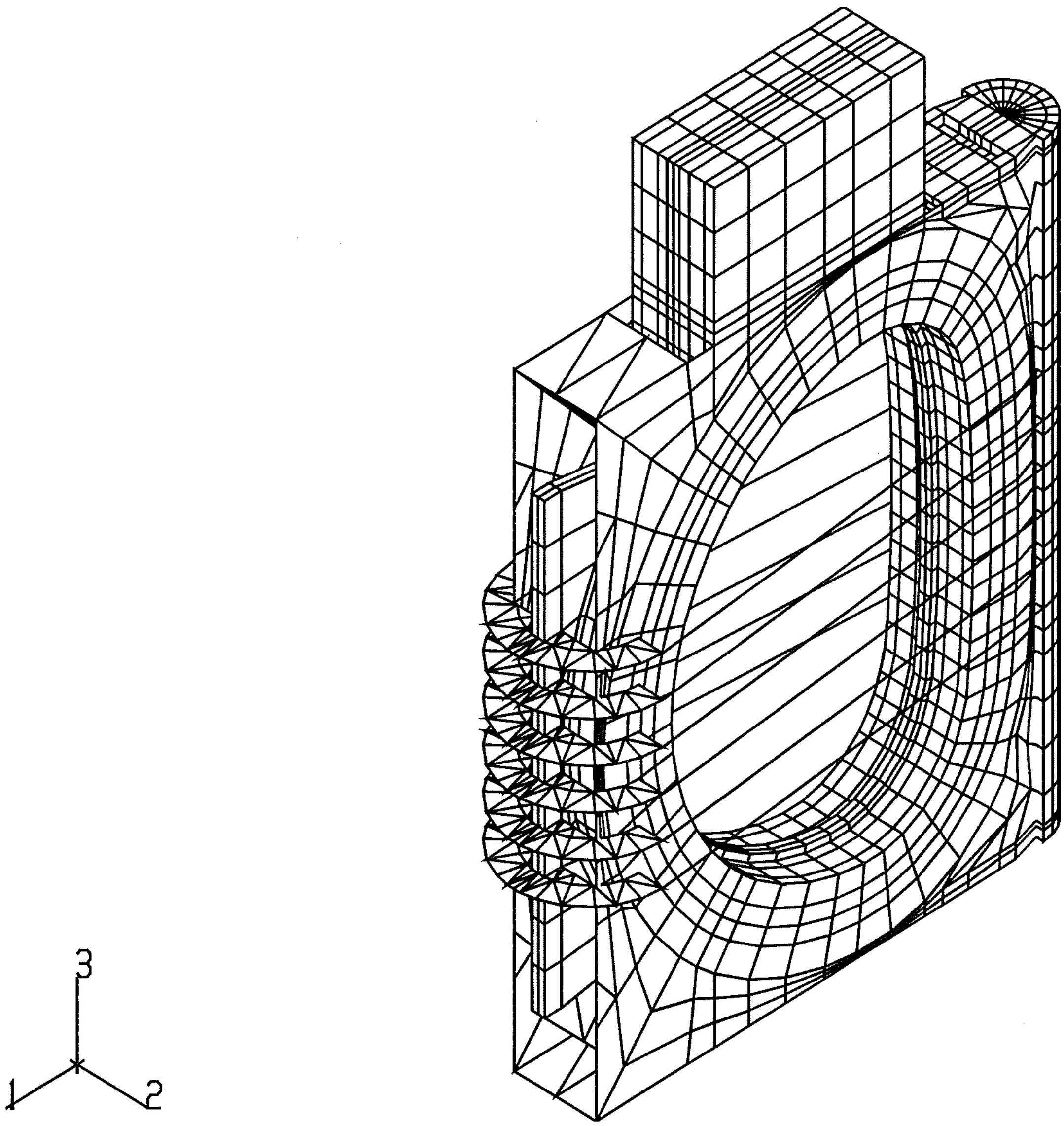

Figure 3 - FE model of the LCT coil

The choice of elements and the material behaviour of the LCT coil are described in detail in the report /3/. The model was meshed with 9546 elements, 13501 nodes, and 40044 degrees of freedom.
The link between the intercoil structure and the LCT casing was simulated with the following boundary conditions shown in figure 4:

- Four nodes (z_1 ,z_2, z_3, and z_4) at the bottom of the LCT casing are fixed in z-direction

- All other marked nodes simulate the intercoil structure. All these nodes are subject to a prescribed displacement (**Table 1**)/5/, which simulates the deformation between the LCT and ITER model coil.
  The two vertical lines represent the inner contour of the TFMC coil and the five horizontal lines show the z-positions of the horizontal plates of the intercoil structure.

POINT		X-DISPLACEMENT	Y-DISPLACEMENT	Z-DISPLACEMENT
Node	8716	4.58038E-02	2.35656E+00	-6.51176E-01
Node	8718	1.98461E-01	1.23649E+00	3.7858SE-01
Node	9145	-1.65899E+00	5.50886E+00	1.75246E+00
Node	9149	-1.59202E+00	5.83183E+00	9.93081E-01
Node	9153	-1.57121E+00	5.96131E+00	2.82553E-01
Node	9166	-1.54797E+00	5.97175E+00	-4.24133E-01
Node	9170	-1.55419E+00	5.80503E+00	-1.16437E+00
Node	12105	-2.51613E+00	-3.09450E-01	-9.79467E-01
Node	12189	-3.31962E+00	-2.44497E-02	3.73359E-01
Node	12244	-5.69166E+00	-6.80944E-01	5.25705E-01
Node	12347	-1.28677E+00	5.78687E+00	1.82285E+00
Node	12380	-6.24956E+00	5.25879E-01	7.66121E-02
Node	12483	-1.25219E+00	6.35782E+00	1.05777E+00
Node	12516	-6.43581E+00	2.54630E-01	-3.98420E-01
Node	12619	-1.21368E+00	6.58032E+00	3.36637E-01
Node	12652	-6.28126E+00	-1.62928E-01	-8.70049E-01
Node	12755	-1.18529E+00	6.59563E+00	-3.86736E-01
Node	12788	-5.75937E+00	-7.02626E-01	-1.31685E+00
Node	12891	-1.16146E+00	6.30406E+00	-1.13817E+00
Node	40853	-4.49085E+00	4.71259E-02	1.38191E-01
Node	41853	-4.51742E+00	-4.35872E+00	-7.62324E-01

Table 1

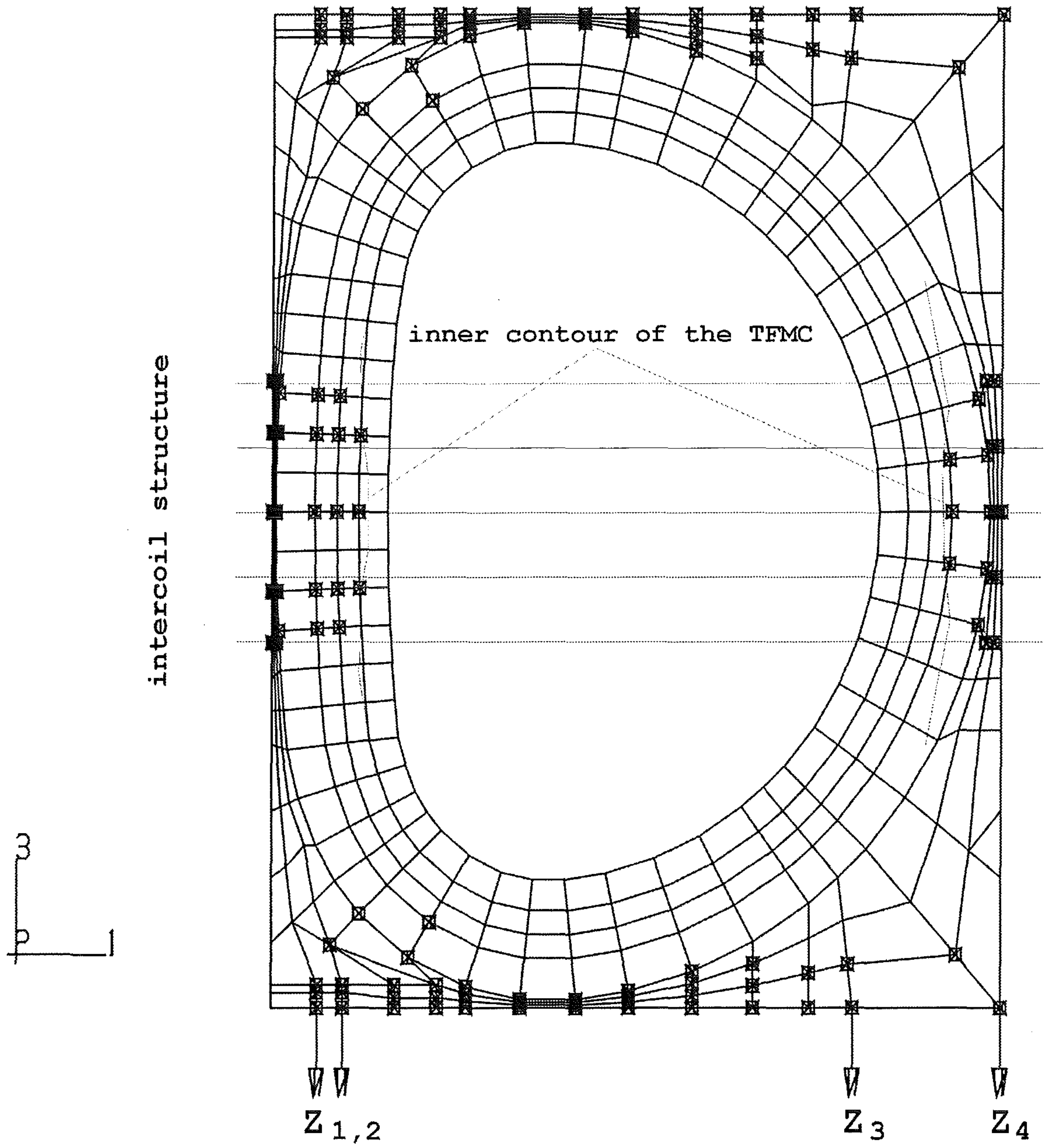

Figure 4 - Boundary conditions in x-, y- and z-direction of the LCT coil

The material behaviour of the **LCT casing** is assumed to be isotropic.

Young's modulus	**E =**	**2.1E+05 MPa**
Poisson's ratio	ν **=**	**0.3**
0.2 strength	$\sigma_{0.2}$ **=**	**1050 MPa (4° K)**

The material behaviour of the **LCT winding** is assumed to be orthotropic and all material data are summarised in Table 2.

critical shear stress τ = 50 MPa

winding radius				
	Young's modulus	R1 front of winding	R2 transition zone	R3 back of winding
radial	E_r [GPa]	10.0	14.9	2.7
azimuthal	E_φ [GPa]	120.0	120.0	120.0
axial	E_z [GPa]	53.0	53.0	53.0
	Poisson number			
	$\nu_{\varphi r}$	0.298	0.298	0.298
	$\nu_{z\varphi}$	0.126	0.126	0.126
	ν_{rz}	0.145	0.145	0.145
	G modulus			
	$G_{r\varphi}$ [GPa]	21.0	21.0	21.0
	$G_{z\varphi}$ [GPa]	26.0	26.0	26.0
	G_{rz} [GPa]	10.0	10.0	10.0

Table 2

2.3 Results

The presentations of the results are plotted with ABAQUS-Post /4/. In Fig. 5 the distributions of the von Mises stress are illustrated as discrete filled colour levels in a detail view of the structure. Each coloured contour corresponds to a range bounded by the values indicated on the similarly coloured band within the legend. It is difficult to show the stress distribution on the surface of the LCT casing, because there is not such a great variety of the values. On an average, the stresses amount to approximately σ_v**=160 MPa**.

casing	von Mises stress [MPa] σ_v
maximum	1208.0

Table 3 - Casing

$\sigma_{0.2}$ = 1050 MPa (4° K)

The maximum equivalent von Mises stress (Table 3) has the value σ_v**=1208.0 MPa** and is about 15% higher than the strength $\sigma_{0.2}$. The critical regions occur in the front and back part of the casing (figures 5 and 6). In Fig. 6 the von Mises stresses σ_v (position line G89) of the LCT casing are plotted over the azimuth angle of the casing.

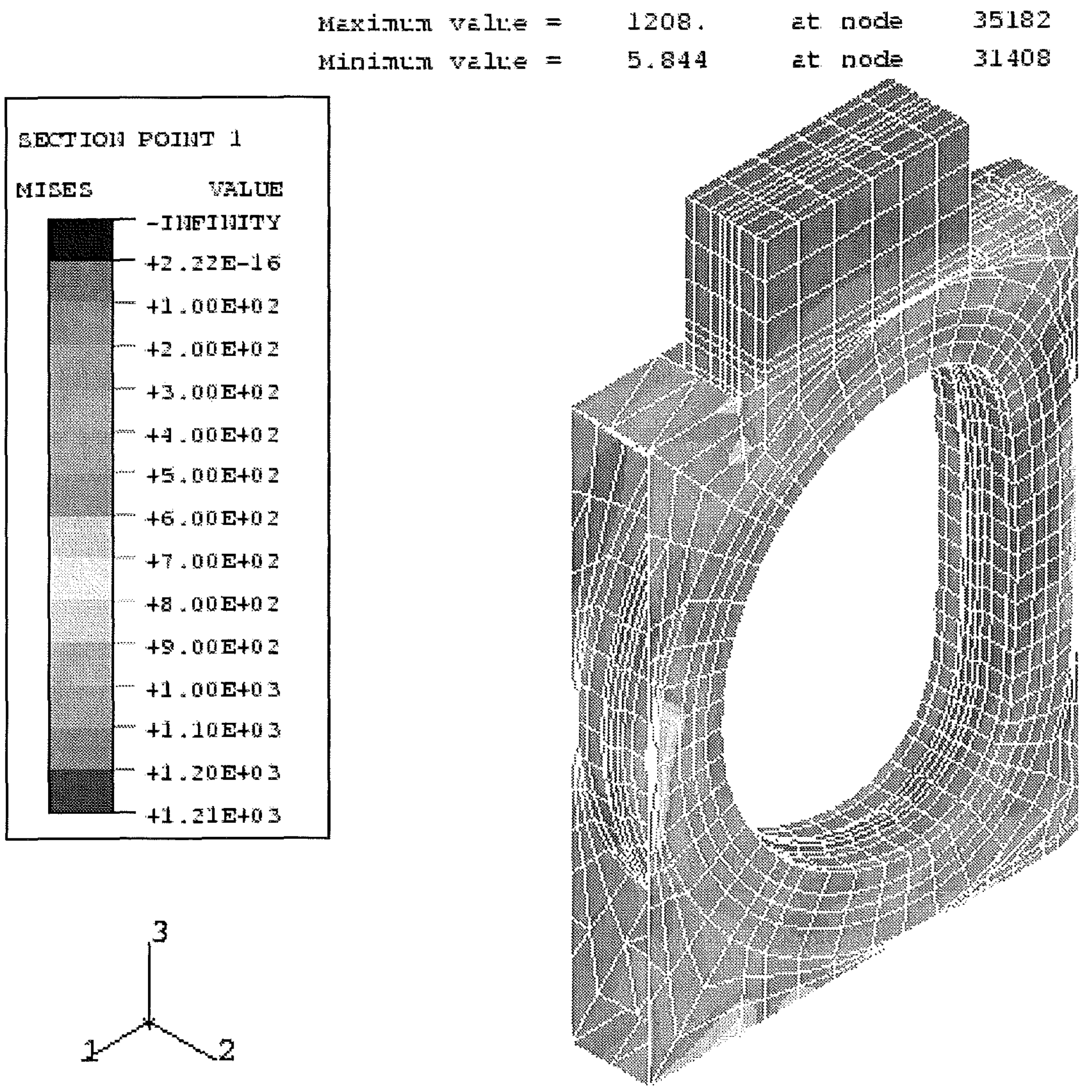

Figure 5 - Contour plot of von Mises stresses in a detail view of the LCT-casing

Figure 7 shows the azimuthal graduation of the structure.

The maximum of the von Mises stresses appears on the position line G89 shown in figures 8 and 9. Two peaks of the stresses σ_v (figures 5 and 6) are found symmetrically at opposite positions at 0.0° (360.0°) **(1208.0 MPa)** and 182.0° **(1056.0 MPa).** These stress peaks are very small and represent superelevations of the stress. According to the principle of St. Venant, the stress values taken at a sufficient distance from the peak position (1 to 2 element lengths) decrease to about **600 MPa**. The von Mises equivalent stresses σ_v are smaller than the strength $\sigma_{0.2}$ by about a factor of **1.75**.

A further stress concentration (figures 5 and 6) appears at the position at 48.3° **(682.70 MPa)** on the side surface in close proximity to the tower.

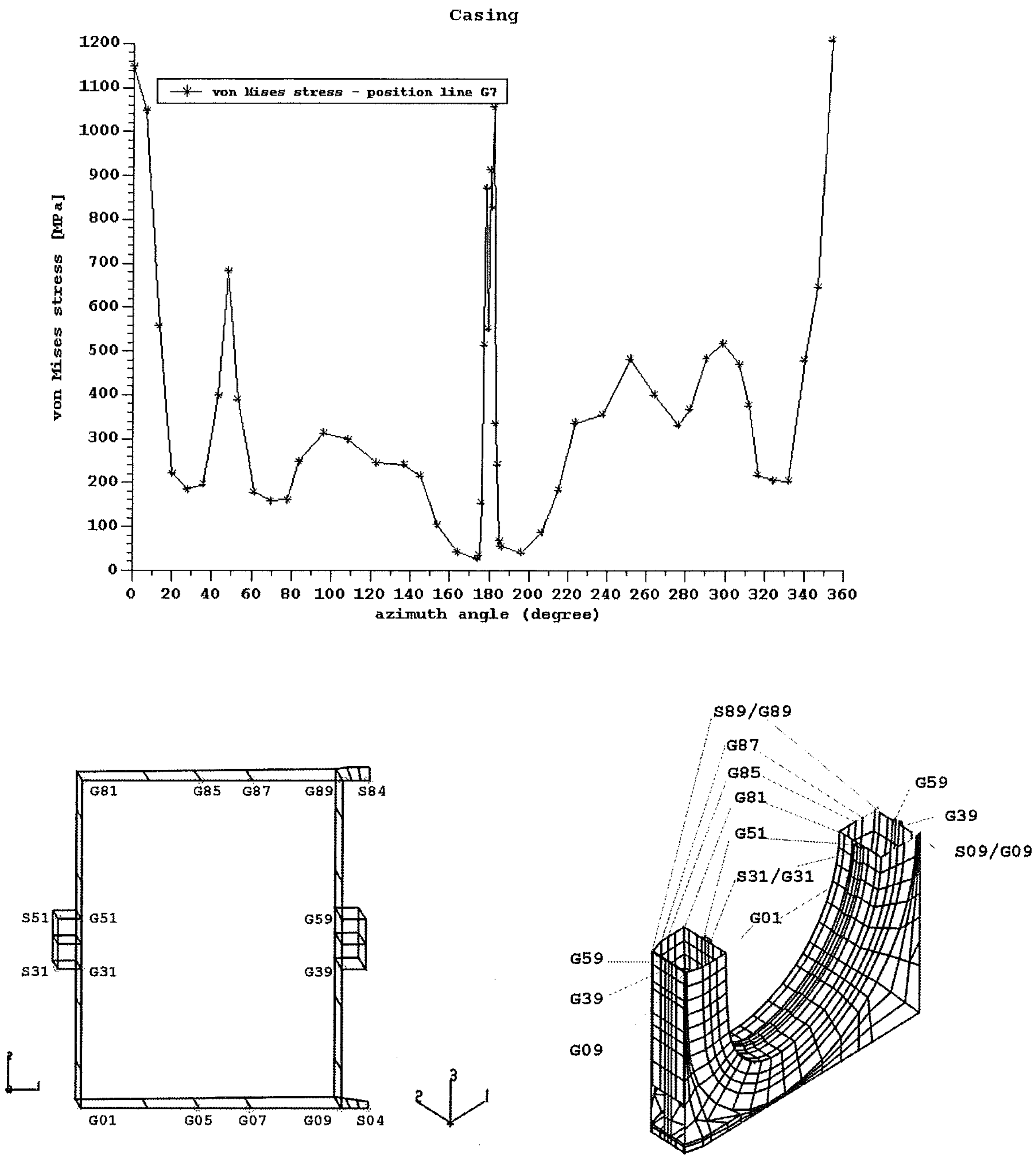

Figure 6 - von Mises stresses of the LCT casing over the azimuth angle

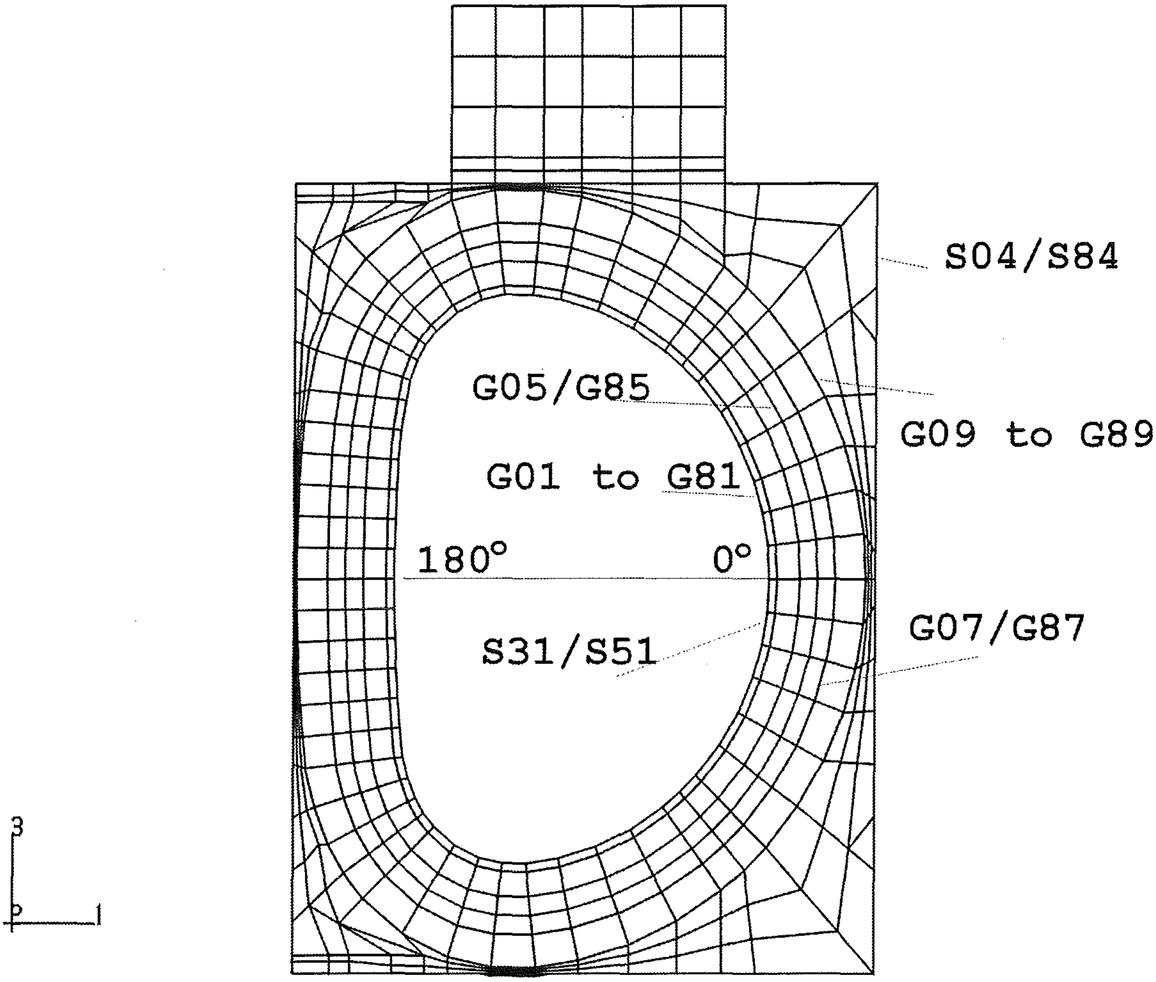

Figure 7 - Azimuthal graduation of the LCT casing and description of the position lines

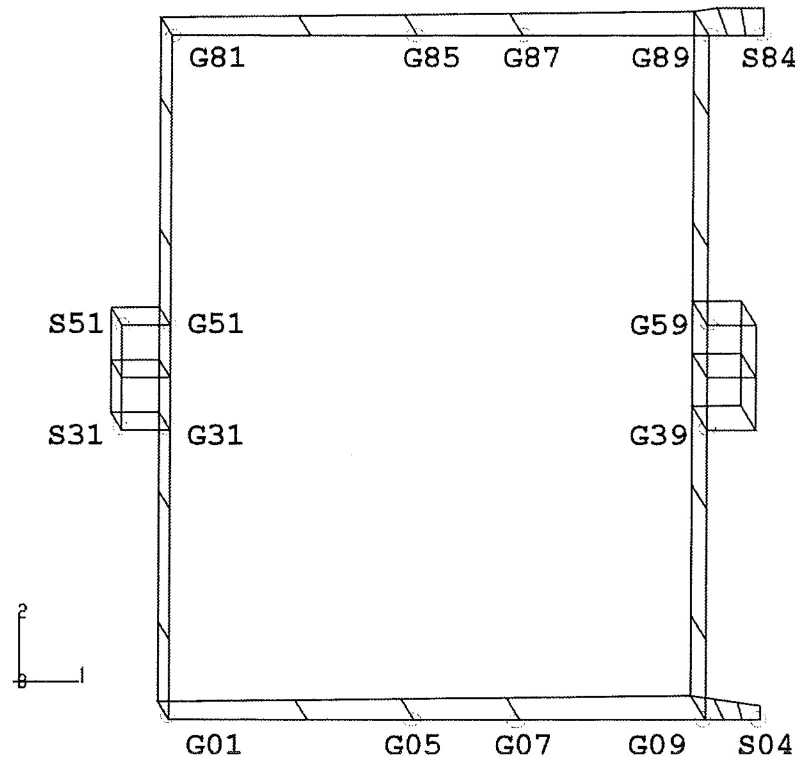

Figure 8 - Cross section of the LCT casing with a description of the position lines

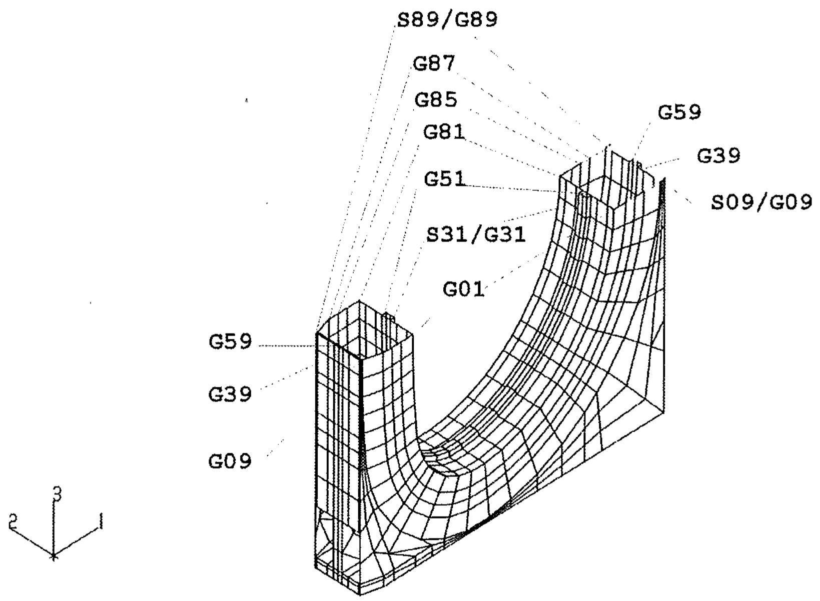

Figure 9 - Lower half of the LCT casing with a description of the position lines

The maximum shear stresses of the LCT winding are summarised in tables 4 and 5.

winding	normal stress [MPa] σ_r	σ_z	σ_φ
maximum	**-0.231**	**+59.97**	**+207.8**
minimum	**-33.28**	**-250.8**	**-75.31**

Table 4 - LCT winding

winding	shear stress [MPa] τ_{rz}	$\tau_{\varphi z}$	$\tau_{r\varphi}$
maximum	**+44.45**	**+22.11**	**+27.15**
minimum	**-24.18**	**-31.30**	**-28.21**

Table 5 - LCT winding

critical shear stress τ = 50 MPa

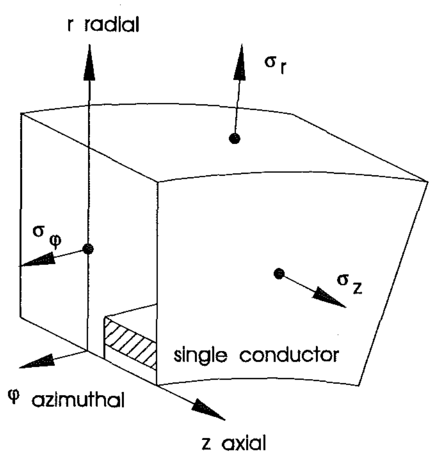

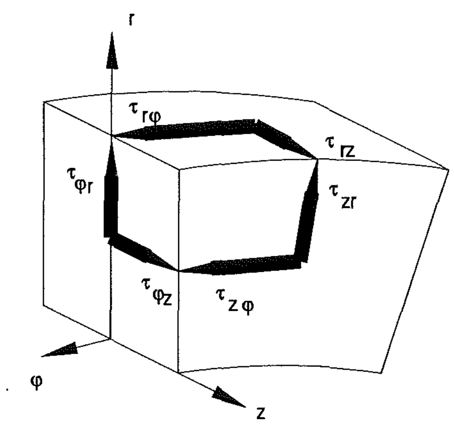

The maximum shear stress of the winding $|\tau_{rz}|$**=44.45 MPa** (table 5) is only 10% below the critical shear stress **τ=50 MPa**. The regions with the maximum stresses are at the outer edge of the winding (figure 10). The other shear stresses are far away from the critical shear stress. They are about 40% smaller than the limit value. Figures 11 and 12 show the stress distributions $\tau_{\varphi z}$ and $\tau_{r\varphi}$. In figures 16, 17, and 18 the shear stresses τ_{rz}, $\tau_{\varphi z}$, and $\tau_{r\varphi}$ of the LCT winding are plotted over the azimuth angle of the winding. The azimuthal graduation of the structure is given in figure 13. The maximum shear stresses τ_{rz} appear on the position lines W79, which can be taken from figures 14 and 15. Both peaks of the shear stresses τ_{rz} are situated about symmetrically at opposite positions of 70° **(44.45 MPa)** and 315° **(41.12 MPa).** They are located above the uppermost and below the lowermost horizontal plate of the intercoil structure. The peaks are very small and decrease by about **15 MPa** at a distance of 1 or 2 element lengths off the peak position. The shear stresses τ then are smaller than the limit value about a factor of **1.6**.

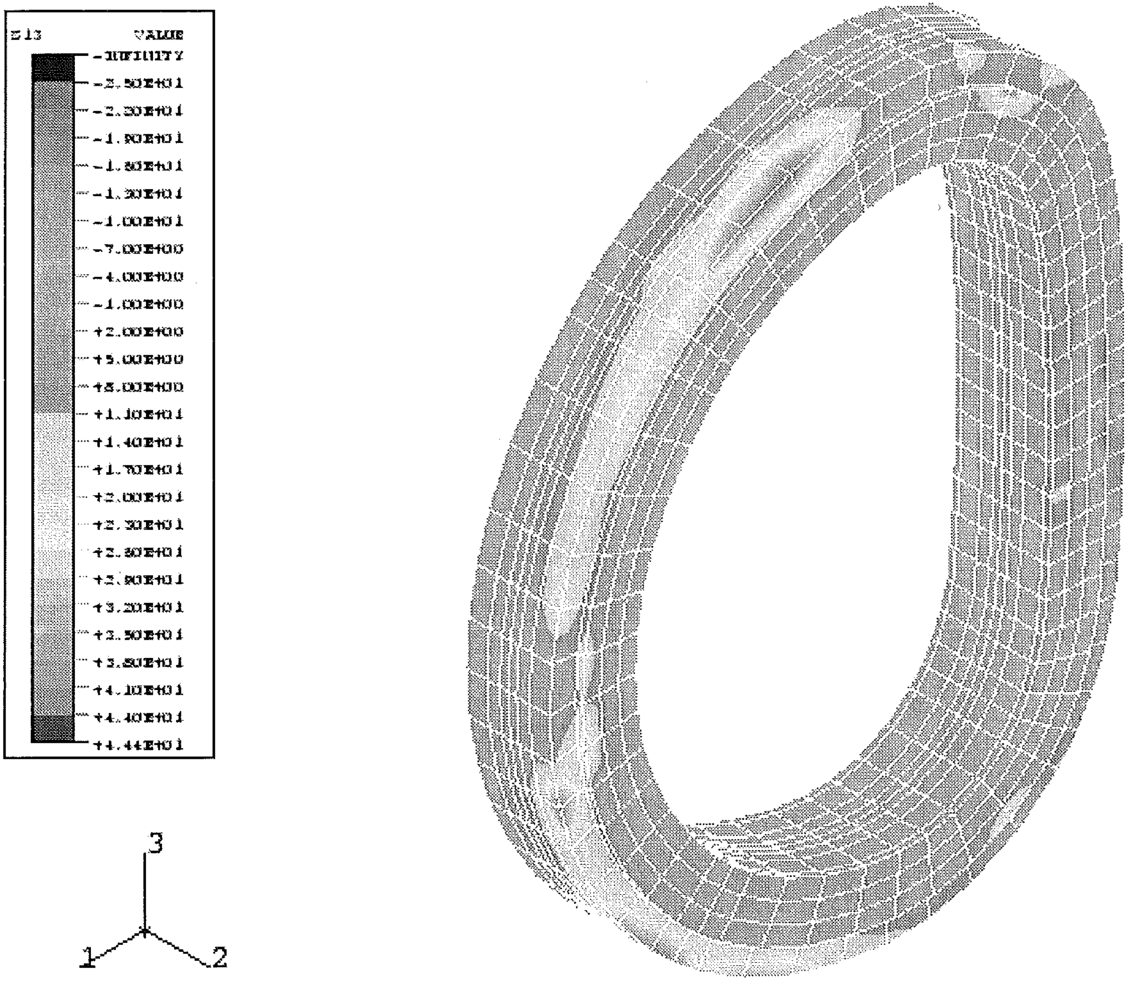

Figure 10 - Contour plot of shear stresses τ_{rz} of the LCT winding

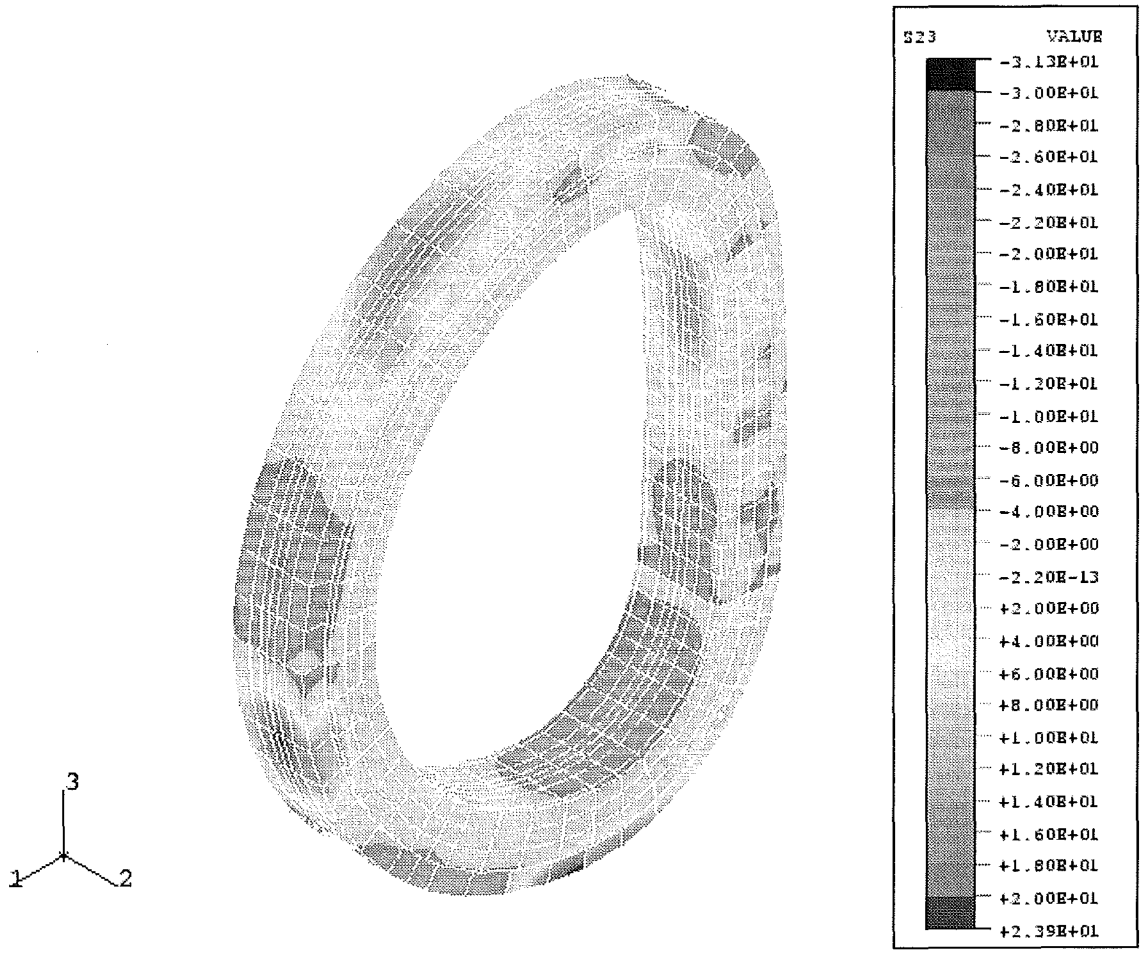

Figure 11 - Contour plot of shear stresses $\tau_{\varphi z}$ of the LCT winding

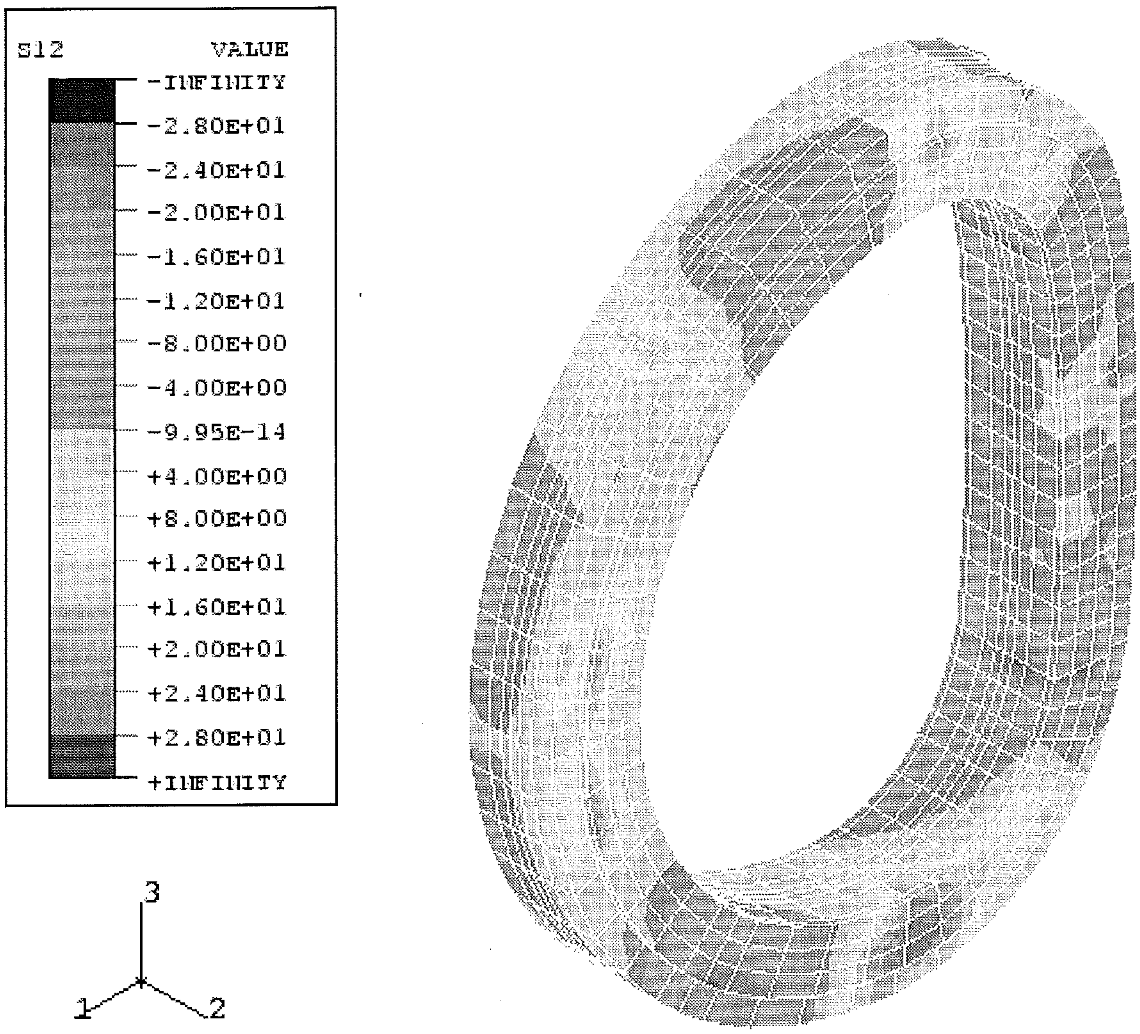

Figure 12 - Contour plot of shear stresses $\tau_{r\varphi}$ of the LCT winding

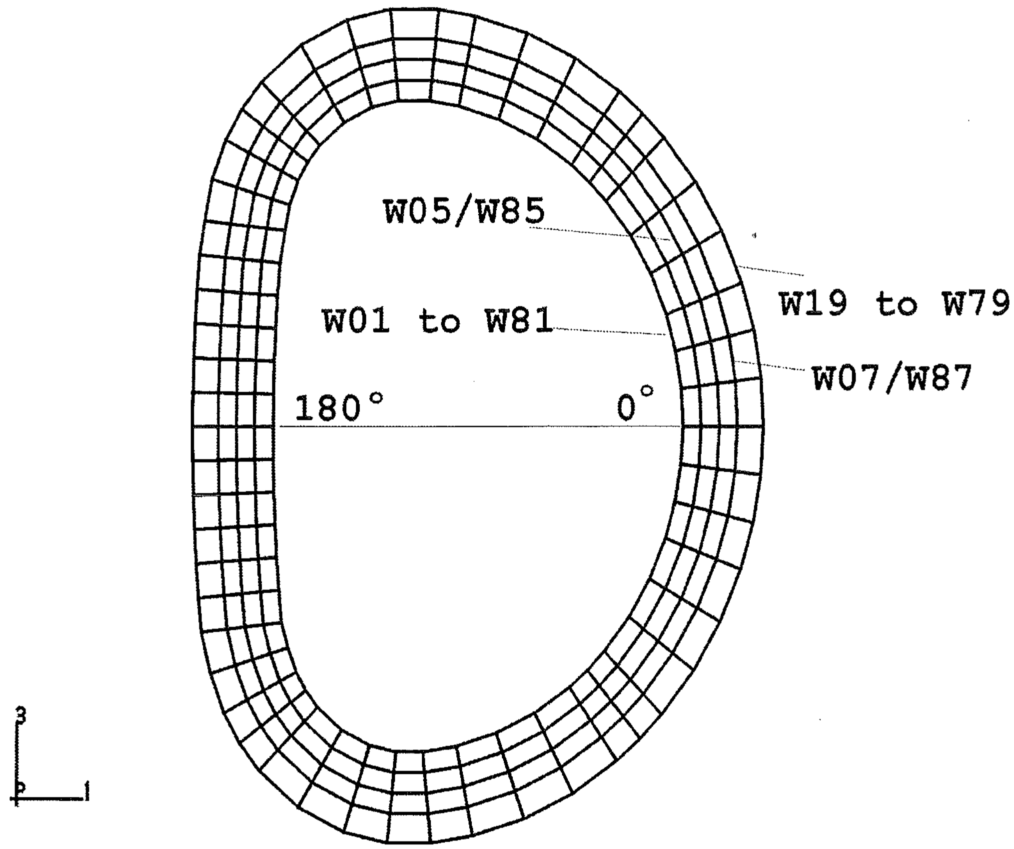

Figure 13 - Azimuthal graduation of the LCT winding and description of the position lines

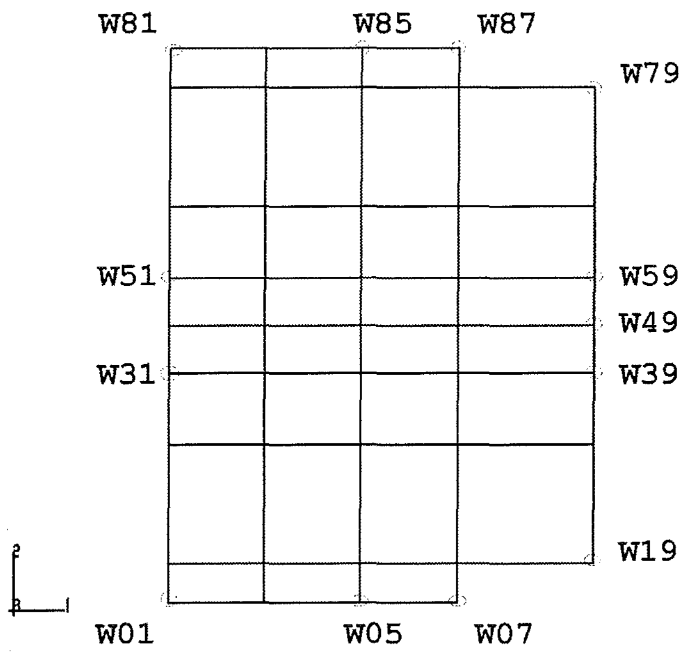

Figure 14 - Cross section of the LCT winding
with a description of the position
lines

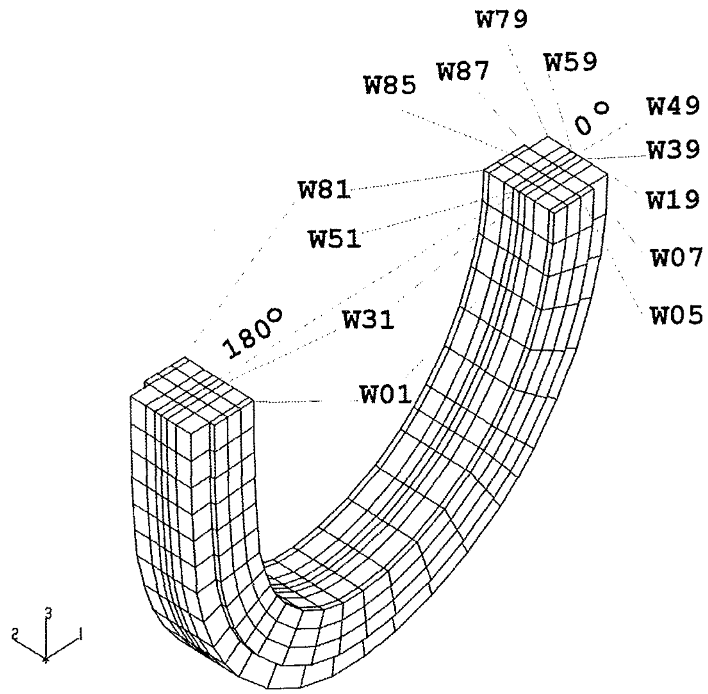

Figure 15 - Lower half of the LCT winding with
a description of the position lines

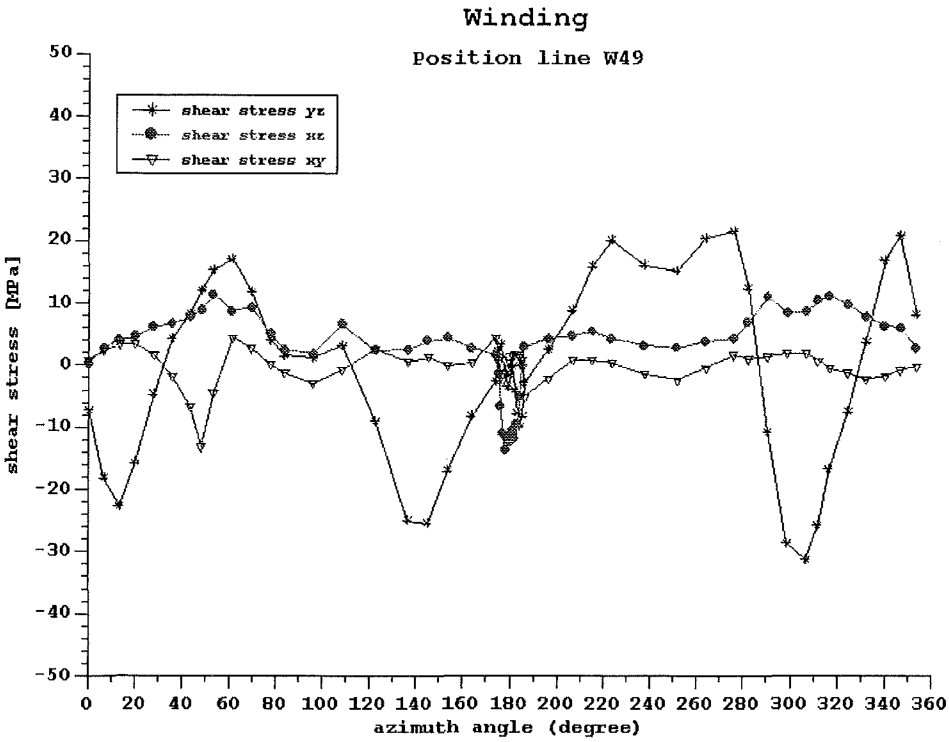

Legend: shear stress xz - τ_{rz}
shear stress yz - $\tau_{\varphi z}$
shear stress xy - $\tau_{r\varphi}$

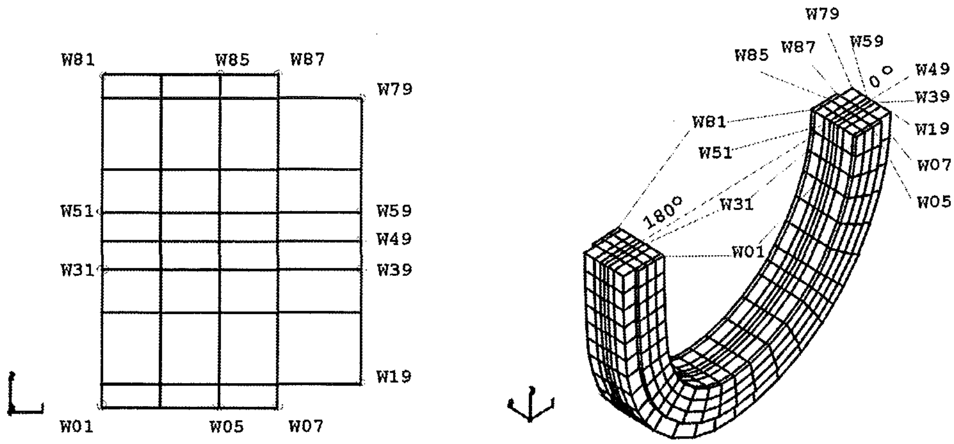

Figure 16 - Shear stresses of the LCT winding over the azimuth angle on the position line W49

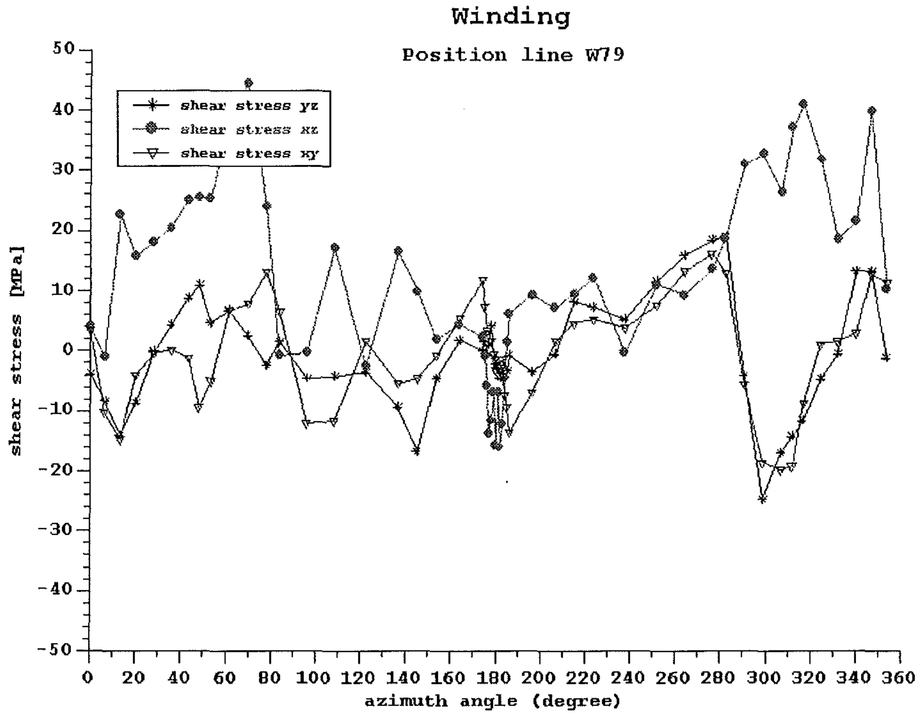

Legend: shear stress xz - τ_{rz}
shear stress yz - $\tau_{\varphi z}$
shear stress xy - $\tau_{r\varphi}$

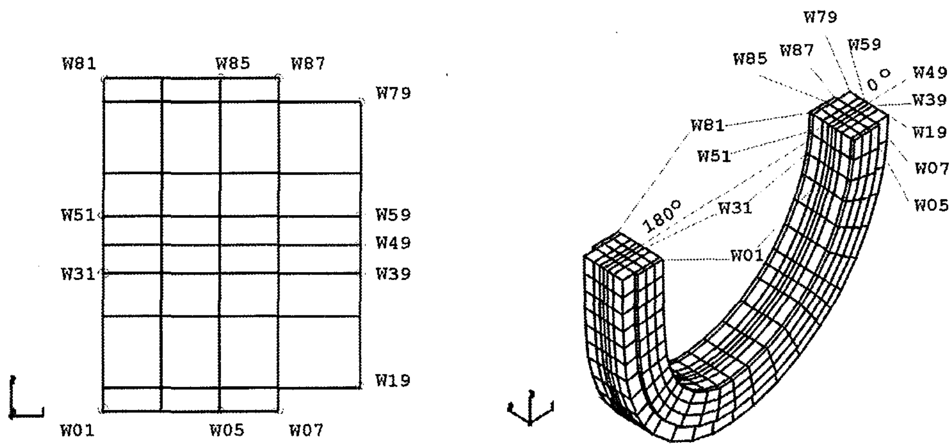

Figure 17 - Shear stresses of the LCT winding over the azimuth angle on the position line W79

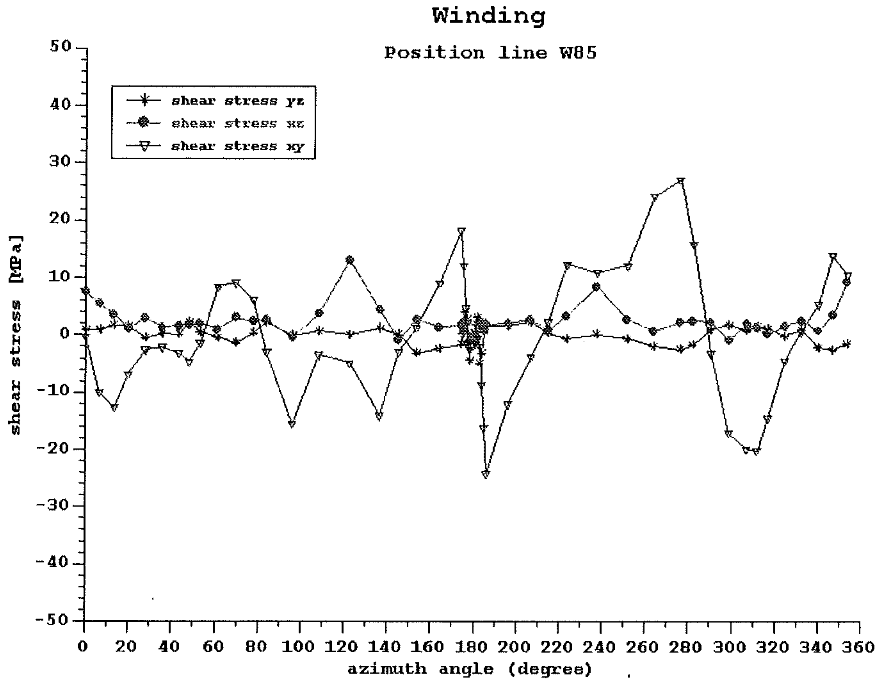

Legend: shear stress xz - τ_{rz}
shear stress yz - $\tau_{\varphi z}$
shear stress xy - $\tau_{r\varphi}$

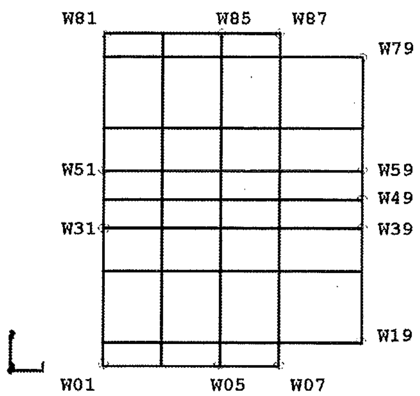

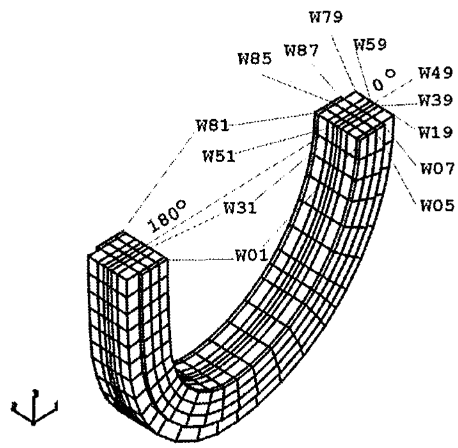

Figure 18 - Shear stresses of the LCT winding over the azimuth angle on the position line W85

The deformations of the casing are presented in figures 19, 20, 21 and 22 in top view, front view and side view, respectively.

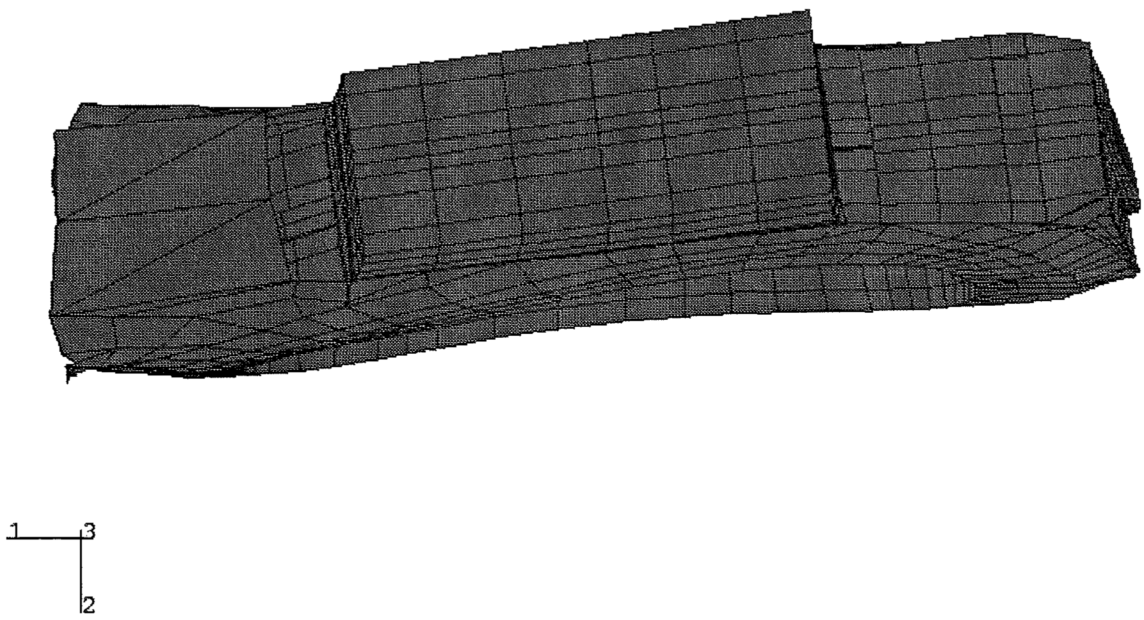

Figure 19 - Top view of the deformed LCT casing

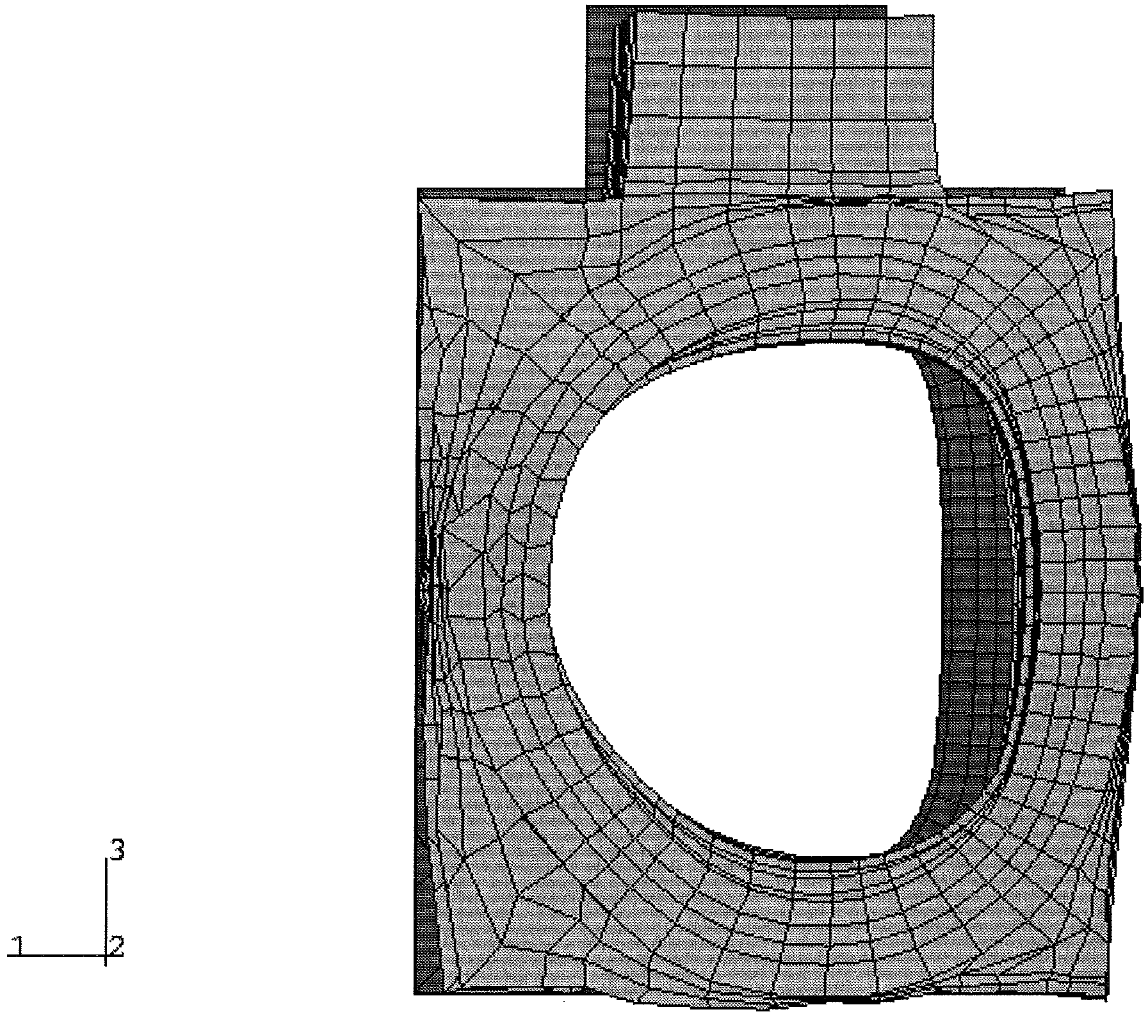

Figure 20 - Front view of the undeformed (red) and deformed (green) LCT casing

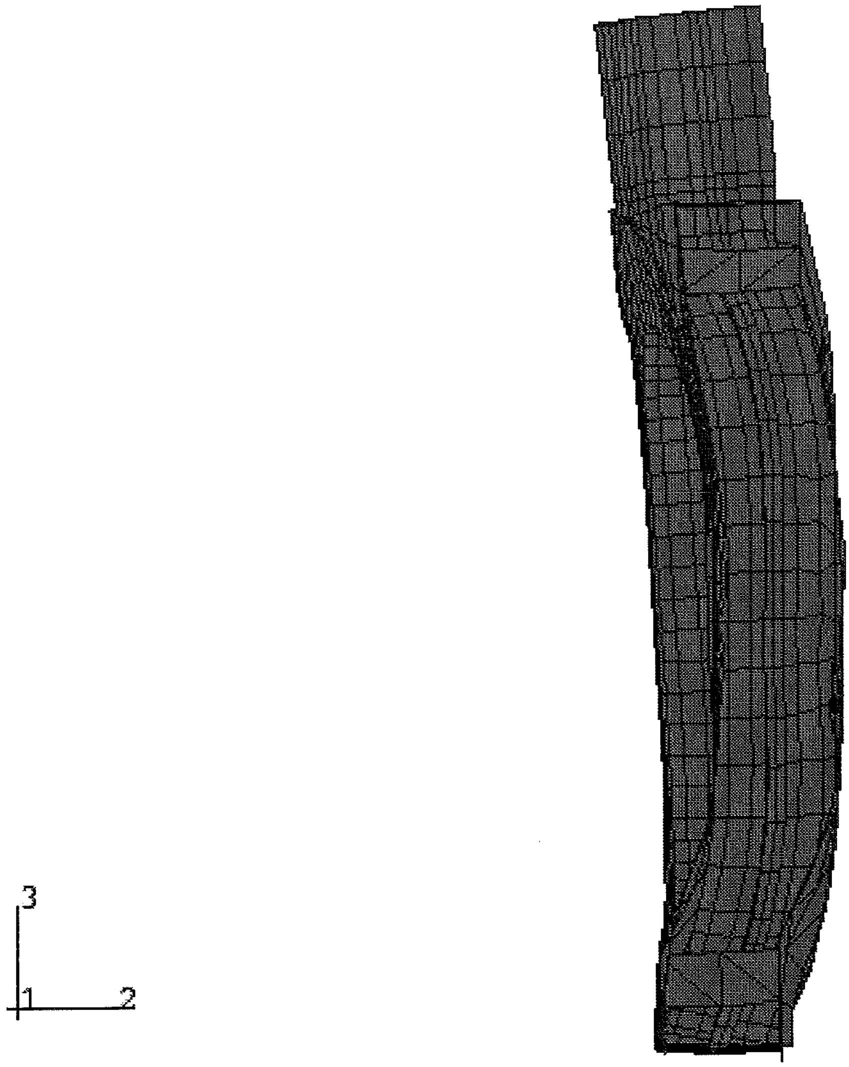

Figure 21 - Side view of the deformed LCT casing

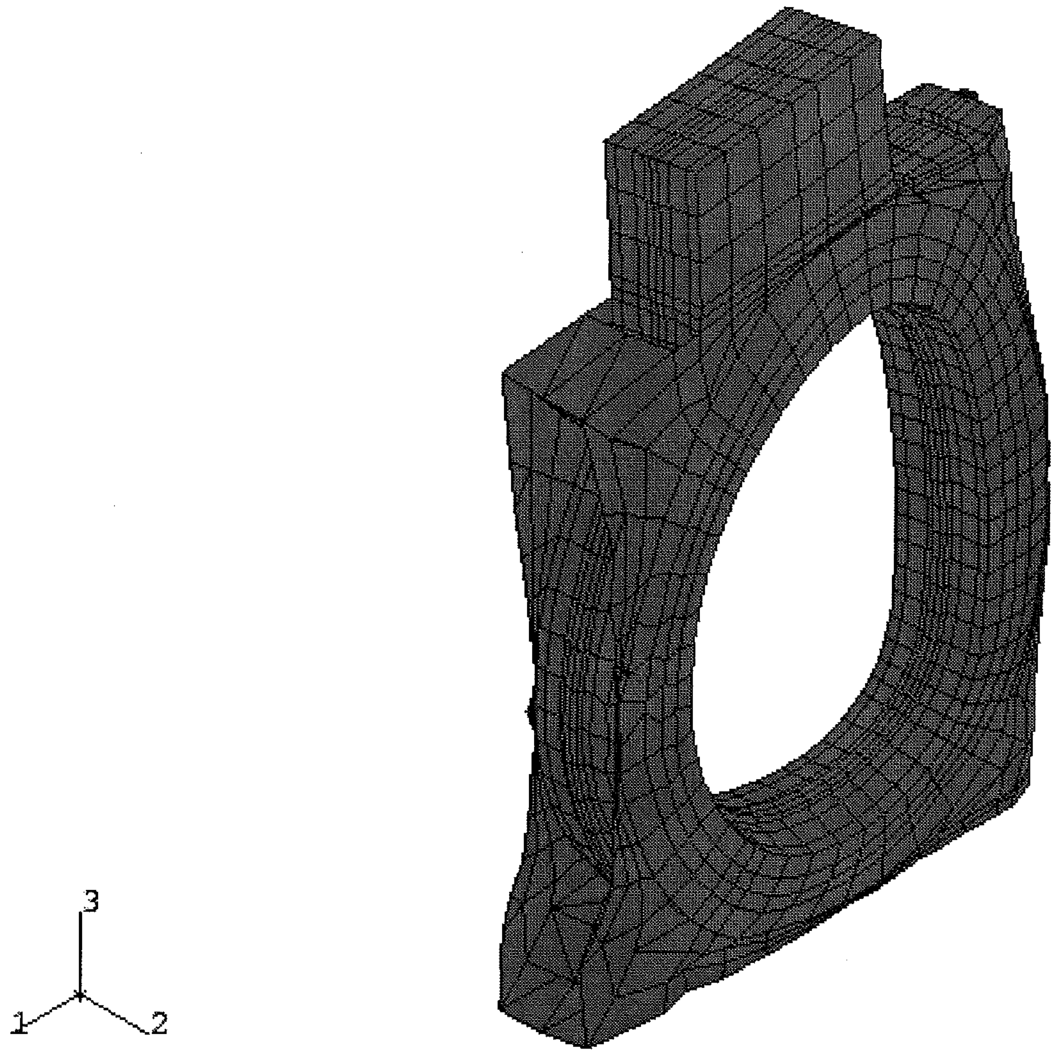

Figure 22 - Isometric view of the deformed LCT casing

In figure 23, the maximum displacements $\mathbf{u_x}$, $\mathbf{u_y}$, and $\mathbf{u_z}$ of the LCT casing are plotted over the azimuth angle of the casing. The maximum displacements are summarised in table 6. The $\mathbf{u_x}$ maximum displacements (+0.199 mm and -6.365 mm) occur at the outer edges of the side wall (position line S84), $\mathbf{u_z}$ (+2.828 mm) in the middle of the inner ring (position line S31) as well as (-2.929 mm) in the middle of the side wall (position line G87), and $\mathbf{u_y}$ (+7.411 mm and -4.676 mm) at the outer edges of the side wall (position line S04) of the LCT casing.

	displacement of the casing					
	$\mathbf{u_x}$ **(mm)**	**angle (°)**	$\mathbf{u_y}$ **(mm)**	**angle (°)**	$\mathbf{u_z}$ **(mm)**	**angle (°)**
max	**+0.199**	**311.75**	**+7.411**	**6.67**	**+2.828**	**0.00**
min	**-6.436**	**180.00**	**-4.676**	**145.00**	**-2.929**	**96.25**

Table 6

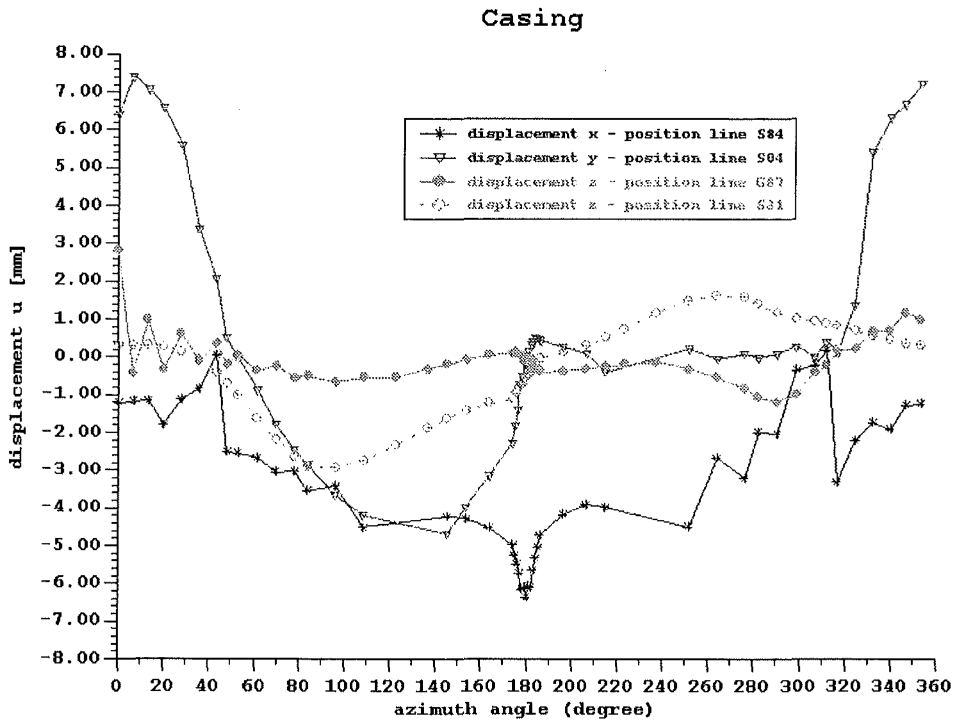

(figure legend: displacements x,y,z correspond to $\mathbf{u}_x, \mathbf{u}_y, \mathbf{u}_z$)

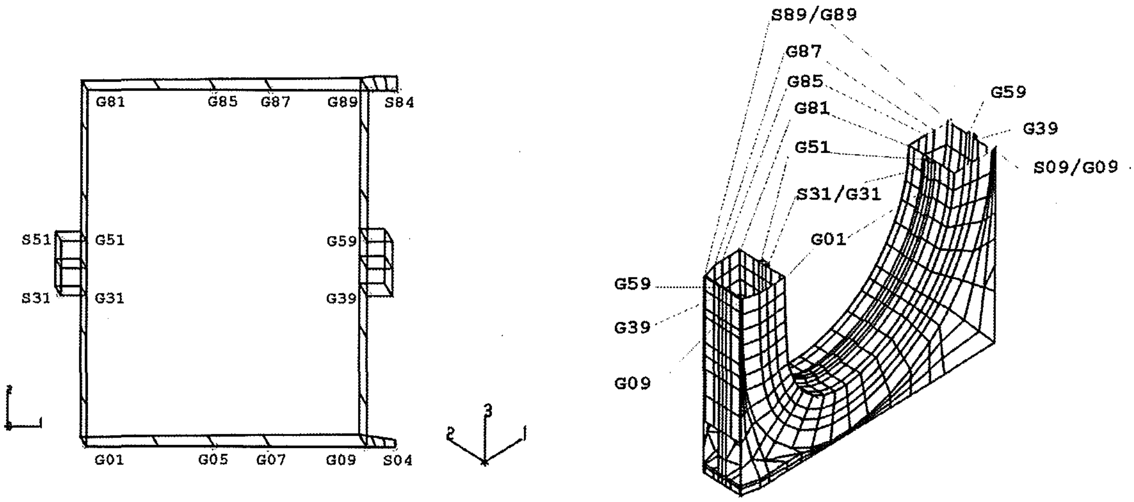

Figure 23 - Displacements of the LCT casing over the azimuth angle

As a result of the radial electromagnetic forces, the LCT coil stretches in x-direction at $\Delta x=6.237$ mm and reduces in z-direction at $\Delta z=5.757$ mm. The deformations are clearly recognisable in figure 20. The prescribed displacements and the out-of-plane forces bend the LCT coil in y-direction (figures 19 and 21). The large displacements are $ymax_1=7.411$ mm and $ymax_2=-4.676$ mm. The maximum displacement in y-direction at $\Delta y=-6.621$ mm is situated at the highest corner of the tower of the LCT coil. This position is marked with "Pmax" in figure 25. All displacements of the LCT casing concerning the position lines S84, S04, and S31 are summarised in tables 7, 8, and 9.

Displacement of the LCT casing position line S84				
node	angle (degree)	u_x (mm)	u_y (mm)	u_z (mm)
30084	0.0000	-1.2140	6.5800	0.3366
30184	6.6667	-1.1850	7.0990	0.2825
30284	13.3333	-1.1610	6.4710	-0.0187
30384	20.0000	-1.8010	6.0960	-0.1721
30484	27.8333	-1.1190	5.9030	-0.0109
30584	35.6667	-0.8415	5.0540	-0.9275
30684	43.5000	0.0458	2.3570	-0.6512
30784	48.2500	-2.5160	-0.3095	-0.9795
30884	53.0000	-2.5580	-0.3095	-0.6078
30984	61.3333	-2.6810	-0.9700	-0.3789
31084	69.6667	-3.0440	-1.6400	-0.4333
31184	78.0000	-3.0400	-2.3100	-0.4490
31284	84.0000	-3.5520	-2.9800	-0.7509
31384	96.2500	-3.4160	-3.6500	-0.5694
31484	108.5000	-4.5170	-4.3590	-0.7623
31784	145.0000	-4.2260	-4.4010	-0.2567
31884	153.5000	-4.2630	-3.8720	0.0625
31984	163.7500	-4.5050	-3.1140	0.2748
32084	174.0000	-4.9790	-2.2370	0.3276
32184	175.0000	-5.2520	-1.7880	0.3320
32284	176.0000	-5.4830	-1.3660	0.2859
32384	177.0000	-5.7290	-0.7026	0.2479
32484	178.0000	-6.1560	-0.1629	0.0389
32584	179.0000	-6.1150	-0.1411	-0.1032
32684	180.0000	-6.3650	0.2546	-0.4098
32784	181.0000	-6.0620	0.1392	-0.2928
32884	182.0000	-6.1080	0.5259	-0.0515
32984	183.0000	-5.6510	0.6809	-0.4976
33084	184.0000	-5.3330	0.5449	-0.6090
33184	185.0000	-5.0430	0.5124	-0.6817
33284	186.0000	-4.7240	0.4475	-0.7099
33384	196.2500	-4.1850	0.2875	-0.6935
33484	206.5000	-3.9180	0.1797	-0.4837
33584	215.0000	-3.9780	-0.0730	-0.1515
33884	251.5000	-4.4910	0.0471	0.1382
33984	263.7500	-2.6690	0.0300	-0.7515
34084	276.0000	-3.2080	0.0200	-0.5809
34184	282.0000	-1.9840	0.0100	-1.1460
34284	290.3333	-2.0400	0.0000	-1.0670
34384	298.6667	-0.3339	-0.0100	-0.6969
34484	307.0000	-0.1849	-0.0245	0.4044
34584	311.7500	0.1985	1.2360	0.3786
34684	316.5000	-3.3200	-0.0245	0.3734
34784	324.3333	-2.2280	-0.0960	-0.1365
34884	332.1667	-1.7410	5.7910	1.0070
34984	340.0000	-1.9130	5.8180	0.9863
35084	346.6667	-1.2870	5.9360	1.2460
35184	353.3333	-1.2520	6.8020	1.3940

Table 7

Displacement of the LCT casing position line S04

node	angle (degree)	u_x (mm)	u_y (mm)	u_z (mm)
30004	0.0000	-0.0586	6.4190	0.0070
30104	6.6667	-0.7830	7.4110	0.0665
30204	13.3333	-0.4551	7.0720	-0.2793
30304	20.0000	-0.1682	6.5980	-0.3483
30404	27.8333	-0.0648	5.6060	-0.4482
30504	35.6667	-0.3434	3.3890	-0.5995
30604	43.5000	-0.2309	2.0660	-0.7653
30704	48.2500	-0.5509	0.5238	-1.0160
30804	53.0000	-1.0260	-0.0530	-1.3970
30904	61.3333	-1.1440	-0.8798	-1.7070
31004	69.6667	-1.2940	-1.7820	-1.9130
31104	78.0000	-1.4610	-2.4520	-2.1610
31204	84.0000	-1.6250	-2.8440	-2.2460
31304	96.2500	-1.7980	-3.6440	-2.3080
31404	108.5000	-2.0420	-4.1980	-2.1640
31704	145.0000	-2.7950	-4.6760	-1.2590
31804	153.5000	-3.1520	-3.9720	-1.1250
31904	163.7500	-3.5710	-3.1400	-1.1180
32004	174.0000	-3.8910	-2.2630	-1.1220
32104	175.0000	-3.9900	-1.8080	-1.1000
32204	176.0000	-4.0720	-1.3940	-1.0610
32304	177.0000	-4.2220	-0.7050	-0.9514
32404	178.0000	-4.2650	-0.5061	-0.9109
32504	179.0000	-4.3400	-0.1912	-0.8315
32604	180.0000	-4.3650	-0.0119	-0.7859
32704	181.0000	-4.3710	0.1559	-0.7463
32804	182.0000	-4.3300	0.3522	-0.6890
32904	183.0000	-4.2940	0.3996	-0.6588
33004	184.0000	-4.1680	0.5233	-0.5566
33104	185.0000	-4.0920	0.4934	-0.5082
33204	186.0000	-4.0050	0.4261	-0.4741
33304	196.2500	-3.7120	0.2727	-0.4632
33404	206.5000	-3.2900	0.1012	-0.4519
33504	215.0000	-2.9940	-0.3943	-0.3354
33804	251.5000	-2.3690	0.2166	0.8512
33904	263.7500	-2.2490	-0.0535	1.0660
34004	276.0000	-2.1630	0.0880	1.2860
34104	282.0000	-1.9750	-0.0324	1.2400
34204	290.3333	-1.8710	0.0740	1.2970
34304	298.6667	-1.8310	0.2765	0.9730
34404	307.0000	-1.9690	0.0080	0.8109
34504	311.7500	-1.8620	0.4197	0.0000
34604	316.5000	-2.0910	0.1428	0.0000
34704	324.3333	-1.3680	1.3650	-0.3695
34804	332.1667	-0.6746	5.4140	0.0500
34904	340.0000	-0.5743	6.3250	0.0466
35004	346.6667	-0.7184	6.6780	0.1996
35104	353.3333	-0.8737	7.2170	-0.1237

Table 8

Displacement of the LCT casing position line S31

node	angle (degree)	u_x (mm)	u_y (mm)	u_z (mm)
30031	0.0000	-0.3807	6.0670	0.3073
30131	6.6667	-0.1750	5.8750	0.3077
30231	13.3333	-0.0244	5.6340	0.3031
30331	20.0000	0.0265	5.3320	0.2683
30431	27.8333	-0.0763	4.8970	0.1527
30531	35.6667	-0.3359	4.3540	-0.0803
30631	43.5000	-0.7114	3.7140	-0.4397
30731	48.2500	-0.9622	3.2800	-0.7156
30831	53.0000	-1.2180	2.8200	-1.0310
30931	61.3333	-1.6360	1.9630	-1.6130
31031	69.6667	-1.9600	1.0860	-2.1820
31131	78.0000	-2.1730	0.2370	-2.6660
31231	84.0000	-2.2780	-0.3212	-2.8990
31331	96.2500	-2.3470	-0.8010	-2.9290
31431	108.5000	-2.4510	-1.0910	-2.7470
31531	122.5000	-2.6870	-1.2780	-2.3450
31631	136.5000	-3.0880	-1.3150	-1.8850
31731	145.0000	-3.4080	-1.2730	-1.6270
31831	153.5000	-3.7540	-1.1840	-1.4100
31931	163.7500	-4.1690	-1.0280	-1.2200
32031	174.0000	-4.5370	-0.8198	-1.1080
32131	175.0000	-4.9380	-0.5466	-0.9733
32231	176.0000	-5.2060	-0.2559	-0.8766
32331	177.0000	-5.3760	-0.0006	-0.7885
32431	178.0000	-5.4820	0.2388	-0.7039
32531	179.0000	-5.5330	0.4556	-0.6213
32631	180.0000	-5.5380	0.6741	-0.5405
32731	181.0000	-5.4940	0.8804	-0.4622
32831	182.0000	-5.4090	1.0920	-0.3847
32931	183.0000	-5.2740	1.2870	-0.3057
33031	184.0000	-5.0820	1.4620	-0.2214
33131	185.0000	-4.8180	1.5830	-0.1323
33231	186.0000	-4.4400	1.6690	-0.0330
33331	196.2500	-4.0820	1.7240	0.1223
33431	206.5000	-3.6680	1.7790	0.3090
33531	215.0000	-3.3290	1.8200	0.5147
33631	223.5000	-3.0250	1.8620	0.7507
33731	237.5000	-2.6590	1.9440	1.1580
33831	251.5000	-2.4520	2.0620	1.4960
33931	263.7500	-2.3680	2.2200	1.6310
34031	276.0000	-2.3240	2.4450	1.5970
34131	282.0000	-2.2700	2.8260	1.4100
34231	290.3333	-2.1850	3.3640	1.1810
34331	298.6667	-2.0930	3.9840	1.0310
34431	307.0000	-1.9960	4.6360	0.9354
34531	311.7500	-1.9290	4.9980	0.8929
34631	316.5000	-1.8340	5.3270	0.8255
34731	324.3333	-1.6310	5.7830	0.6966
34831	332.1667	-1.3720	6.0930	0.5569
34931	340.0000	-1.0950	6.2550	0.4429
35031	346.6667	-0.8480	6.2730	0.3669
35131	353.3333	-0.6129	6.2050	0.3256

Table 9

In figures 24, 25, and 26, the displacement distributions of the LCT casing, $\mathbf{u_x}$, $\mathbf{u_y}$, and $\mathbf{u_z}$ are plotted in discrete filled colour levels in a detail of the structure. Each coloured contour corresponds to a range bounded by the values indicated on the similarly coloured band within the legend.

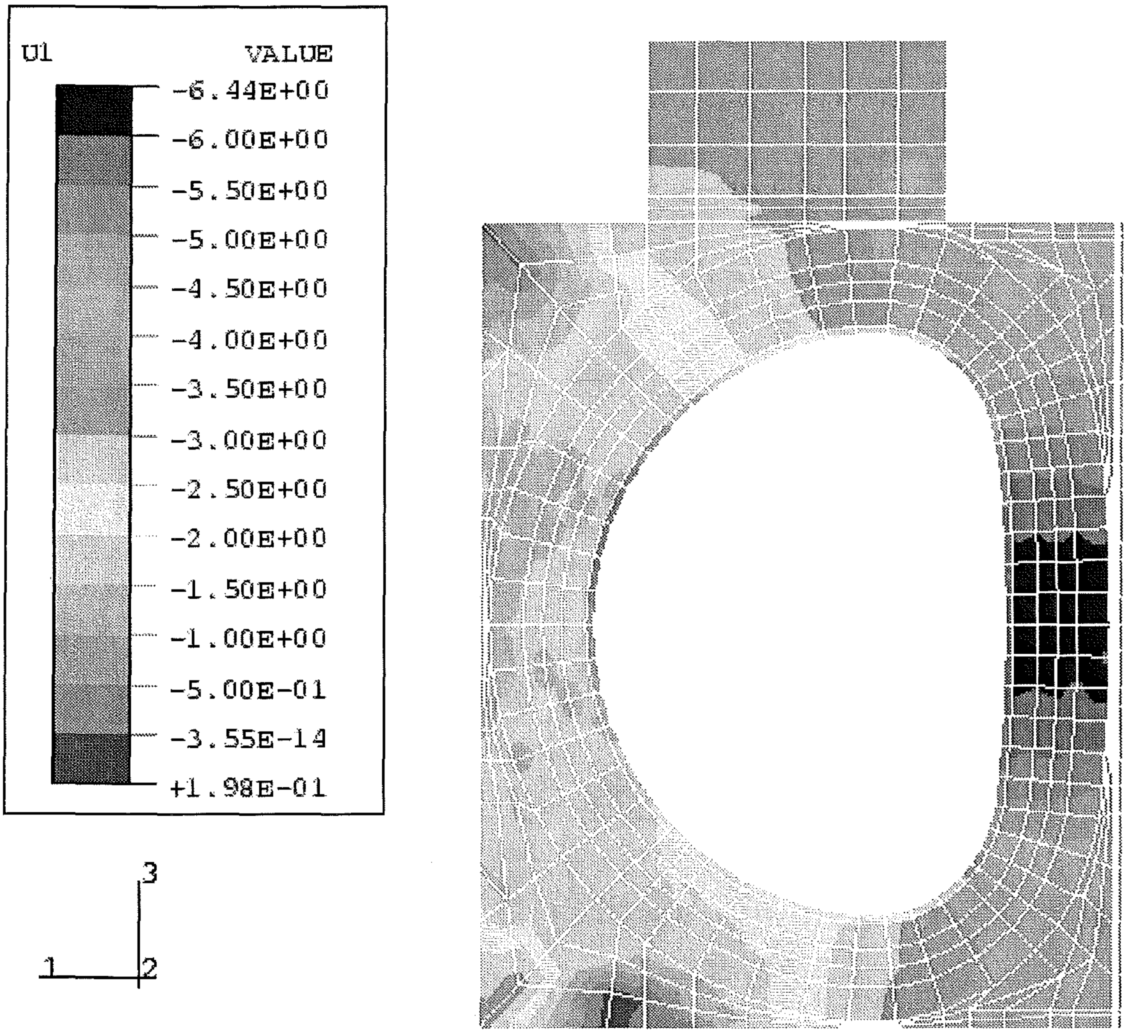

Figure 24 - Contour plot of the displacement $\mathbf{u_x}$ of the LCT casing

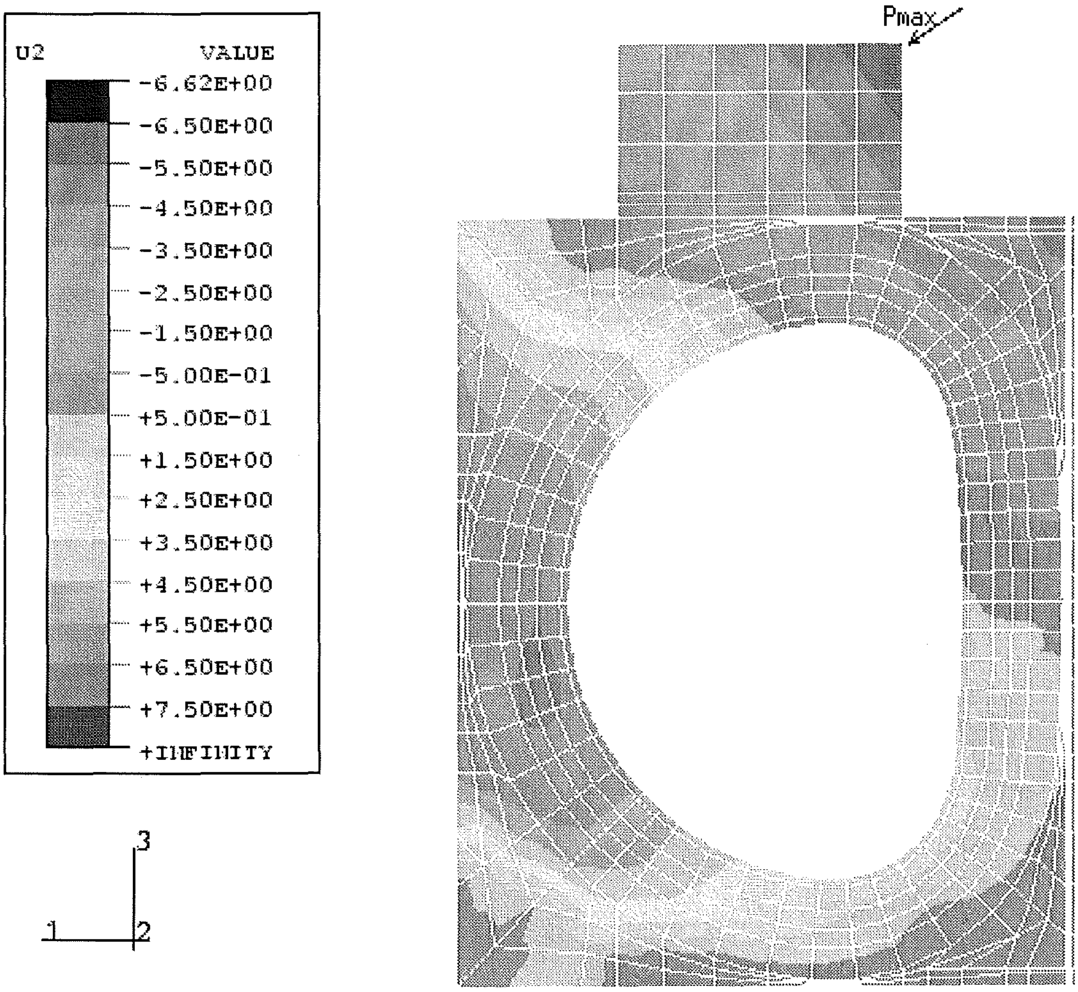

Figure 25 - Contour plot of the displacement u_y of the LCT casing

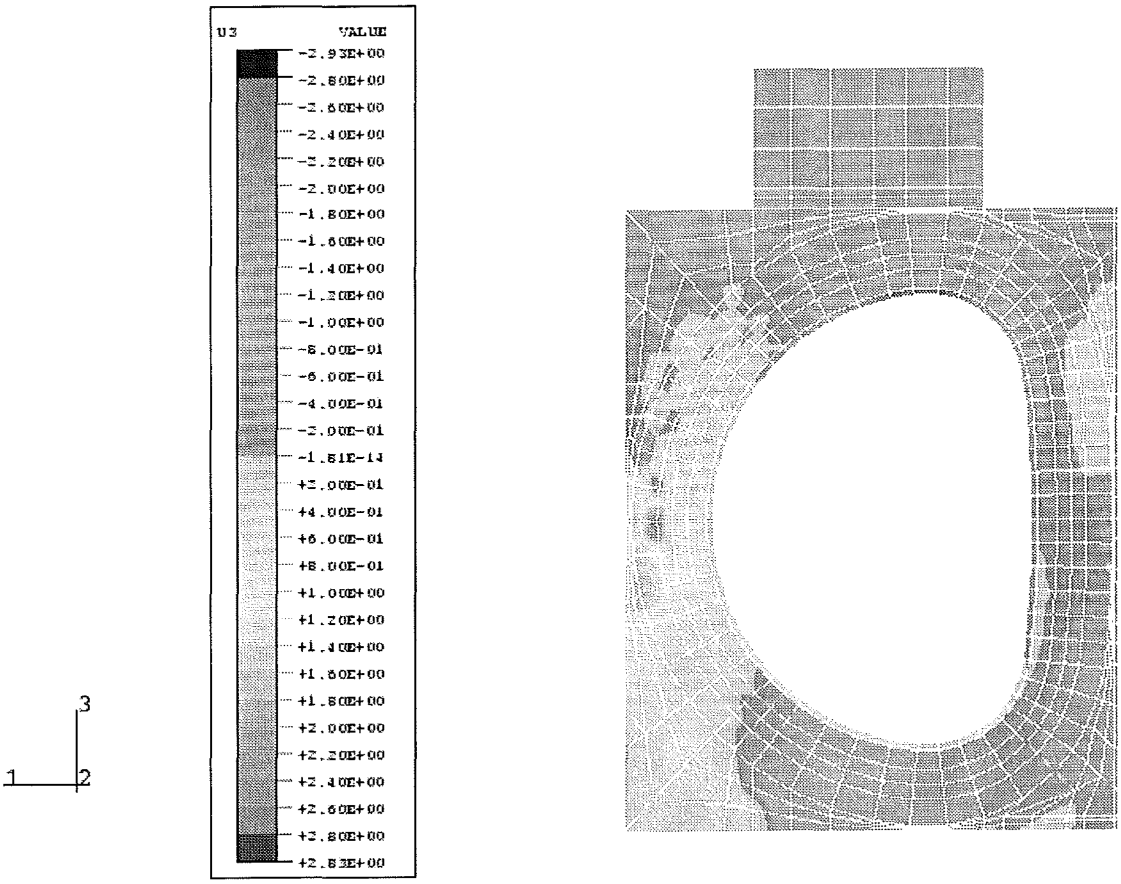

Figure 26 - Contour plot of the displacement u_z of the LCT casing

The deformations of the winding are plotted in figures 27, 28, 29, and 30 in the top view, front view, and side view, respectively.

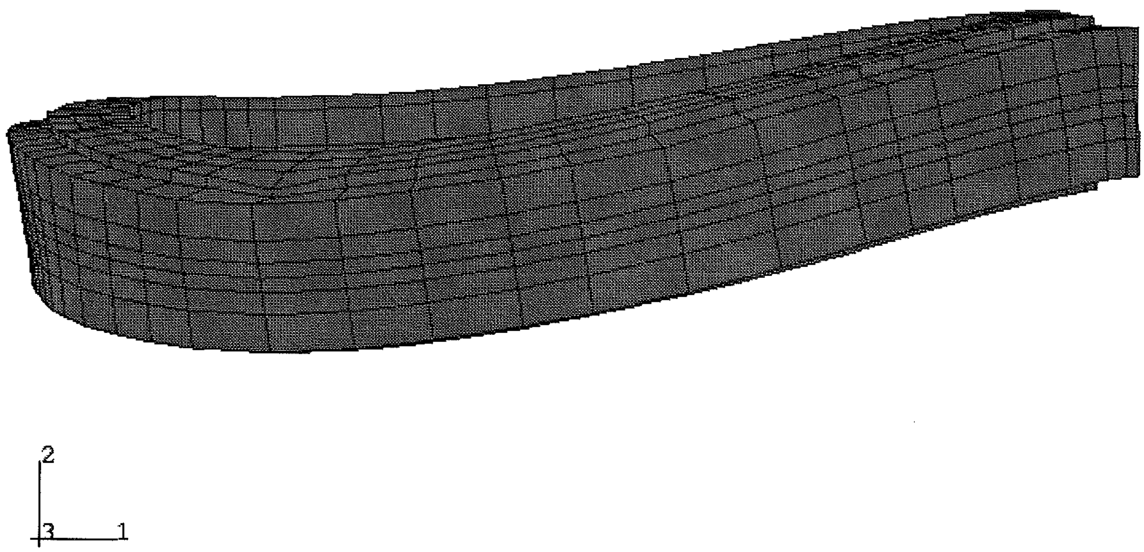

Figure 27 - Top view of the deformed LCT winding

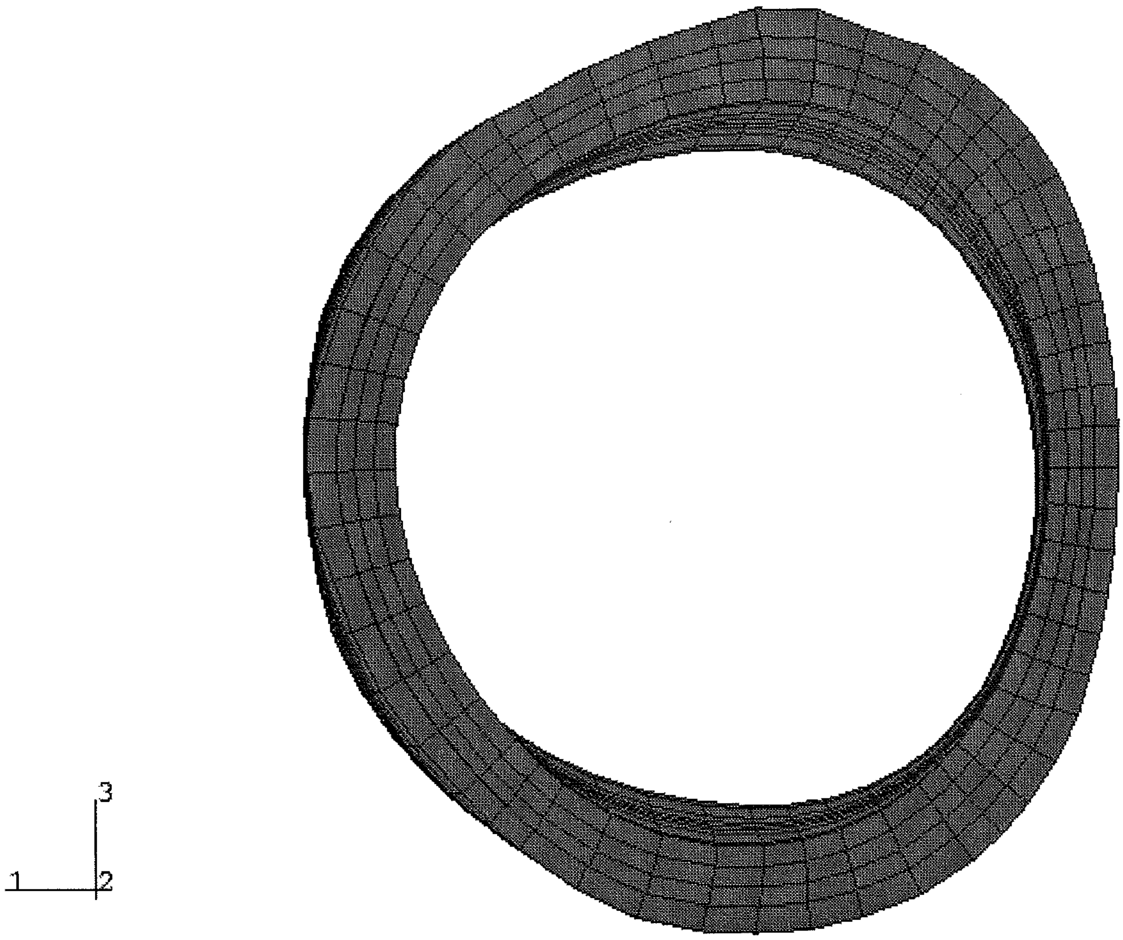

Figure 28 - Front view of the deformed LCT winding

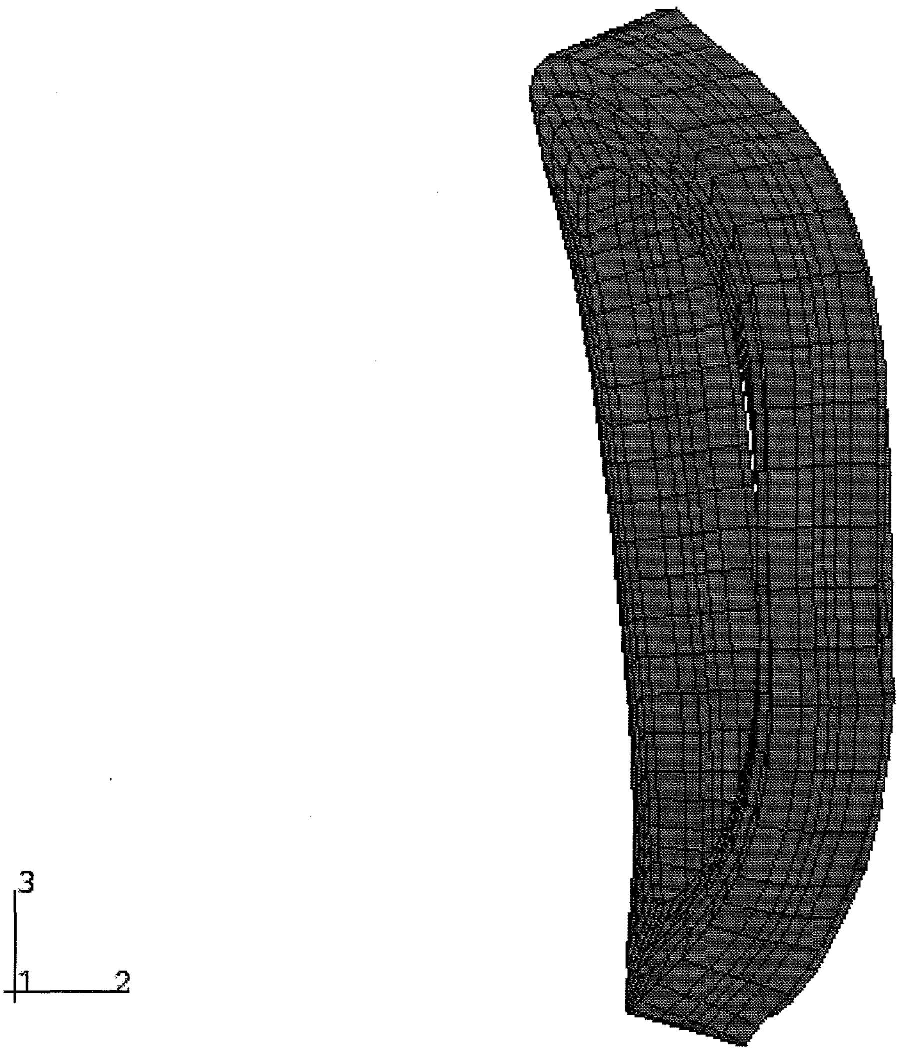

Figure 29 - Side view of the deformed LCT winding

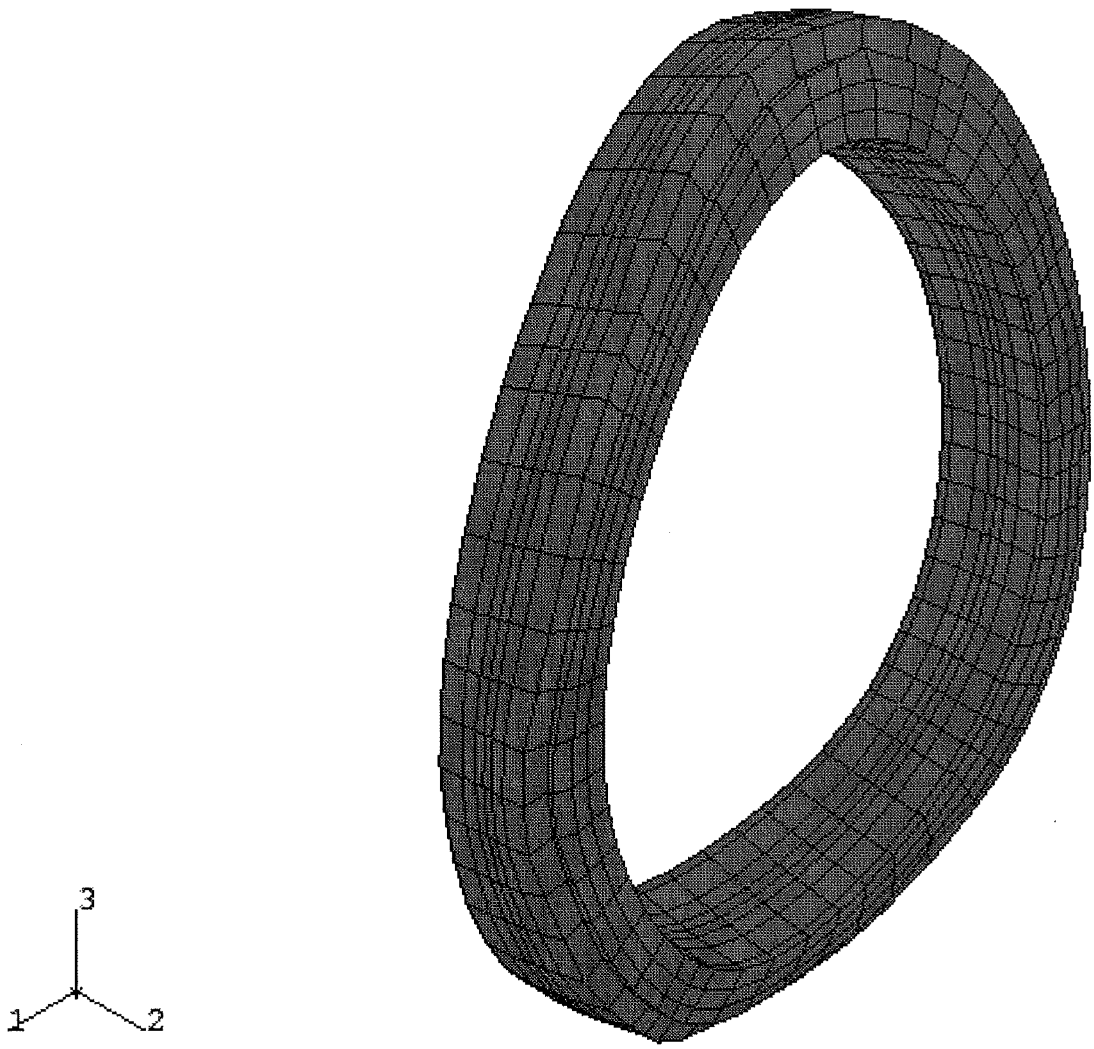

Figure 30 - Isometric view of the deformed LCT winding

The maximum displacement $\mathbf{u_x}$ occurs on the border of the inner ring (position line W81), $\mathbf{u_z}$ on the border of the outer ring (position line W07), and $\mathbf{u_y}$ in the middle of the outer ring (position line W29) of the LCT winding. In figure 31, $\mathbf{u_x}$, $\mathbf{u_y}$, and $\mathbf{u_z}$ of the LCT winding are plotted over the azimuth angle of the winding. The maximum displacements are summarised in table 10.

	displacement of the winding					
	u_x (mm)	**angle (°)**	**u_y (mm)**	**angle (°)**	**u_z (mm)**	**angle (°)**
max	**+0.488**	**27.83**	**+6.606**	**340.00**	**+1.037**	**276.00**
min	**-7.535**	**180.00**	**-4.318**	**122.50**	**-2.001**	**96.25**

Table 10

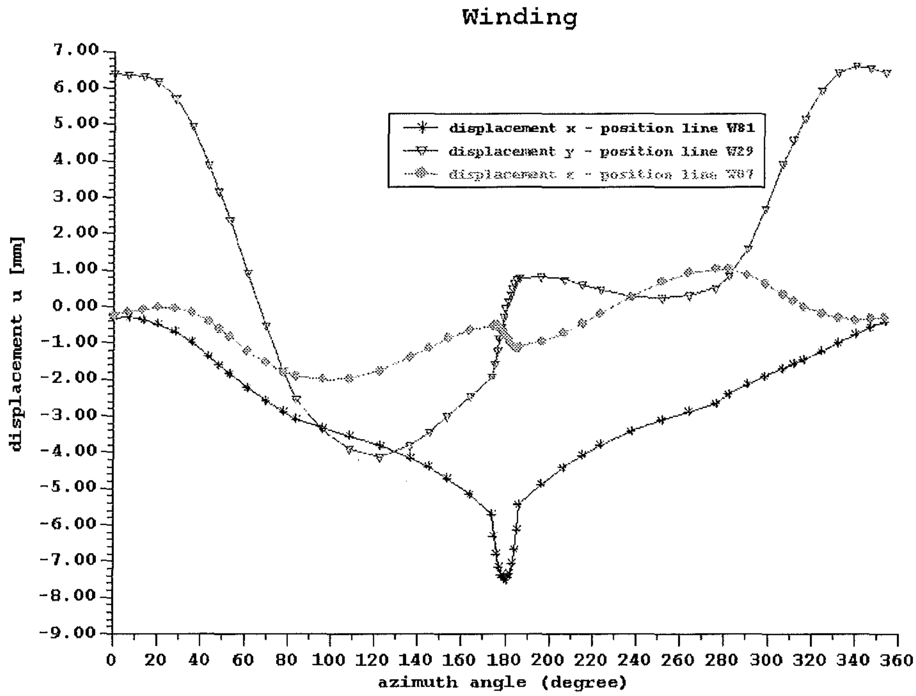

(figure legend: displacements x,y,z correspond to $\mathbf{u}_x,\mathbf{u}_y,\mathbf{u}_z$)

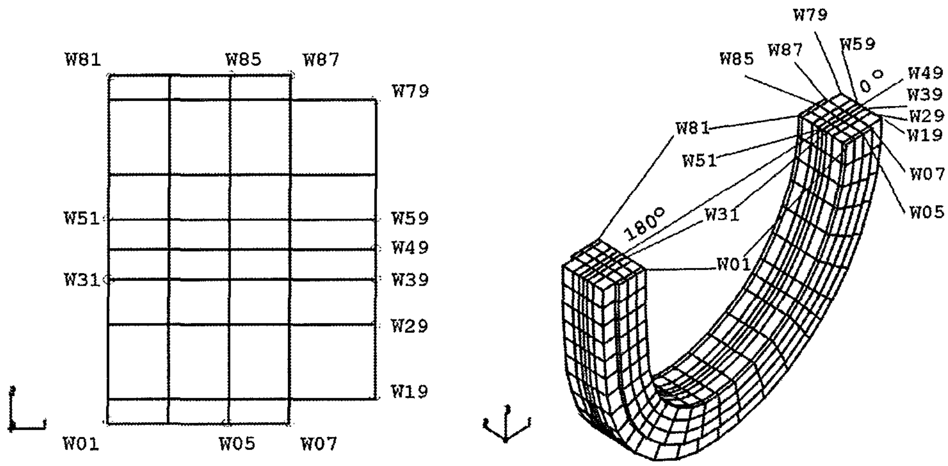

Figure 31 - Displacements of the LCT winding over the azimuth angle

3. Conclusion

For the test configuration consisting of the LCT coil, the intercoil structure, and the ITER-TF model coil, the estimate with the assumed boundary conditions shows that the stresses in the LCT winding and casing are not so critical. There are some small peaks with high stresses which are reduced rapidly in a distance of 1 or 2 element lengths off the peak position.

4. References

/1/ - S.J. Sackett, UCID 176221 "EFFI - a code for calculating the electromagnetic field, force and inductance in coil systems of arbitary geometry", 1977

/2/ - ABAQUS USER MANUAL, Version 5.4, Hibbitt, Karlson & Sorensen, Inc.

/3/ - A. Grünhagen, unpublished report Kernforschungszentrum Karlsruhe, Oktober 1992

/4/ - ABAQUS/Post Reference Guide Version 5.4, Hibbitt, Karlson & Sorensen, Inc.

/5/ - S. Raff, unpublished report